From the RSNA Refresher Courses

MR Imaging of the Ankle and Foot[1]

Zehava S. Rosenberg, MD • Javier Beltran, MD • Jenny T. Bencardino, MD

Magnetic resonance (MR) imaging has opened new horizons in the diagnosis and treatment of many musculoskeletal diseases of the ankle and foot. It demonstrates abnormalities in the bones and soft tissues before they become evident at other imaging modalities. The exquisite soft-tissue contrast resolution, noninvasive nature, and multiplanar capabilities of MR imaging make it especially valuable for the detection and assessment of a variety of soft-tissue disorders of the ligaments (eg, sprain), tendons (tendinosis, peritendinosis, tenosynovitis, entrapment, rupture, dislocation), and other soft-tissue structures (eg, anterolateral impingement syndrome, sinus tarsi syndrome, compressive neuropathies [eg, tarsal tunnel syndrome, Morton neuroma], synovial disorders). MR imaging has also been shown to be highly sensitive in the detection and staging of a number of musculoskeletal infections including cellulitis, soft-tissue abscesses, and osteomyelitis. In addition, MR imaging is excellent for the early detection and assessment of a number of osseous abnormalities such as bone contusions, stress and insufficiency fractures, osteochondral fractures, osteonecrosis, and transient bone marrow edema. MR imaging is increasingly being recognized as the modality of choice for assessment of pathologic conditions of the ankle and foot.

Abbreviations: PVNS = pigmented villonodular synovitis, STIR = short-inversion-time inversion recovery, 3D = three-dimensional

Index terms: Ankle, anatomy, 46.92 • Ankle, fractures, 46.41 • Ankle, injuries, 46.41, 46.48 • Ankle, MR, 46.1214 • Foot, anatomy, 46.92 Foot, fractures, 46.41 • Foot, injuries, 46.48 • Foot, MR, 46.1214

RadioGraphics 2000; 20:S153–S179

[1]From the Department of Radiology, Hospital for Joint Diseases, NYU Medical Center, 305 E 17th St, New York, NY 10003 (Z.S.R.); the Department of Radiology, Maimonides Medical Center, Brooklyn, NY (J.B.); and the Department of Radiology, Massachusetts General Hospital, Harvard Medical School, Boston, Mass (J.T.B.). Presented as a refresher course at the 1999 RSNA scientific assembly. Received March 22, 2000; revision requested May 23 and received June 30; accepted July 5. **Address correspondence to** Z.S.R. (e-mail: *zehava.rosenberg@usa.net*).

Introduction

The past 15 years have witnessed an explosion of information regarding the role of magnetic resonance (MR) imaging in assessing pathologic conditions of the ankle and foot. MR imaging has revitalized the study of musculoskeletal disease in this anatomic area due to its high soft-tissue contrast resolution and multiplanar capabilities. It provides a quick, noninvasive tool for the diagnosis of related injuries, which are often difficult to diagnose with alternative modalities. MR imaging is particularly advantageous for assessing soft-tissue structures around the ankle such as tendons, ligaments, nerves, and fascia and for detecting occult bone injuries. In this article, we review the normal MR imaging anatomy of the ankle and foot and discuss numerous related soft-tissue and osseous abnormalities that are seen with this modality.

Imaging Technique

Routine ankle MR imaging is performed in the axial, coronal, and sagittal planes parallel to the table top. The foot is imaged in the oblique axial plane (ie, parallel to the long axis of the metatarsal bones), oblique coronal plane (ie, perpendicular to the long axis of the metatarsals), and oblique sagittal plane (Fig 1). The patient is supine with the foot in about 20° of plantar flexion. Plantar flexion is useful for three reasons: it decreases the magic angle effect, it accentuates the fat plane between the peroneal tendons, and it allows better visualization of the calcaneofibular ligament. An extremity surface coil is used to enhance spatial resolution. A wrist coil or other small dedicated coils are often used to evaluate the distal foot. T1-weighted (repetition time msec/echo time msec = 600/20) and T2-weighted (2,000/20,80) MR images are obtained with a 12–16-cm field of view, a 256 × 192–512 acquisition matrix, 1–2 signals acquired, and a 3–5-mm section thickness with 1-mm intervals.

Marrow abnormalities are best evaluated with fat suppression techniques such as fat-suppressed proton-density–weighted imaging or with short-inversion-time inversion recovery (STIR) sequences (1,500/20; inversion time msec = 100–150). However, susceptibility to gradient inhomogeneity makes fat suppression techniques less optimal than STIR techniques in imaging the ankle and foot. Cartilage abnormalities can be visualized with two-dimensional or three-dimensional (3D) gradient-echo sequences.

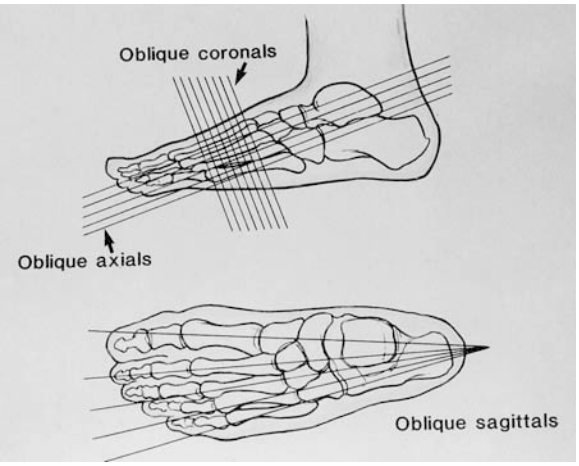

Figure 1. Drawings of the foot illustrate the oblique axial, oblique coronal, and oblique sagittal imaging planes.

Normal Ligamentous Anatomy

Three ligamentous groups support the ankle joint. The syndesmotic ligamentous complex is composed of the anterior and posterior tibiofibular and interosseous ligaments. The lateral collateral ligament is subdivided into the anterior talofibular, posterior talofibular, and calcaneofibular ligaments. The deltoid ligament has five bands: the anterior and posterior tibiotalar ligaments and the tibiospring, tibiocalcaneal, and tibionavicular ligaments.

The ligaments are readily identified as thin, linear, low-signal-intensity structures joining adjacent bones and are usually delineated by contiguous high-signal-intensity fat (1). Heterogeneity is typically seen due to the interposition of fat between the ligamentous fibers. This is particularly true for the anterior tibiofibular ligament, the tibiotalar components of the deltoid ligament, and the posterior talofibular ligament. Axial and coronal imaging with the foot in dorsiflexion and plantar flexion have been recommended to allow visualization of the ligaments in their entirety (2). The ligaments can also be studied with 3D Fourier transform reformatted images (3). In our experience, however, the ligaments can be reliably

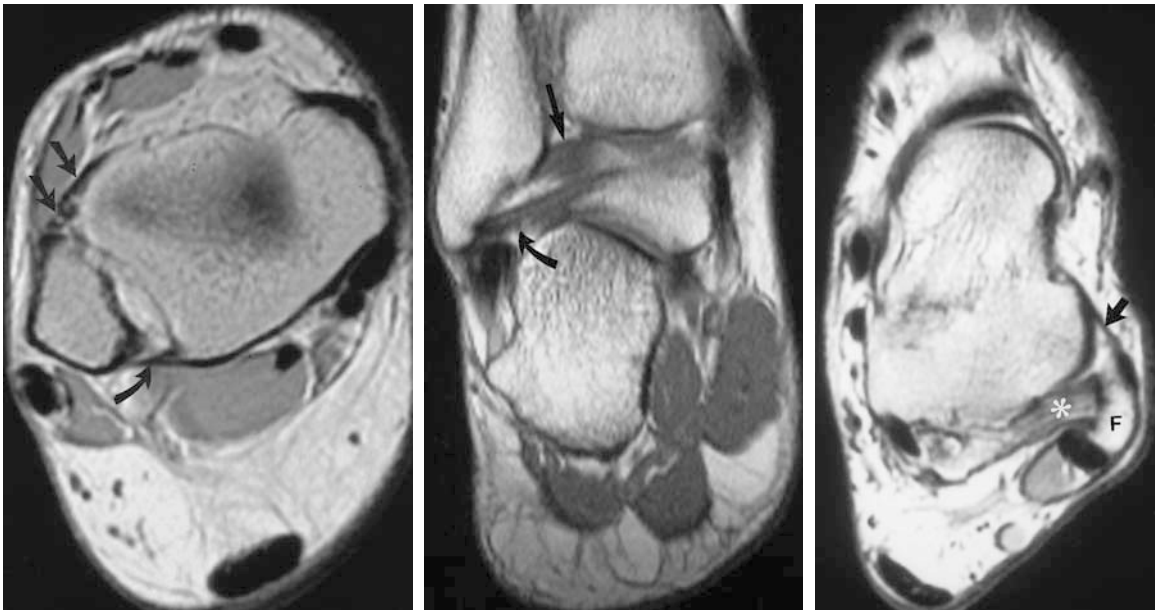

2a. 2b. 3.

Figures 2, 3. **(2)** Normal tibiofibular ligaments. **(a)** Axial T1-weighted MR image obtained at the joint level demonstrates the anterior (straight arrows) and posterior (curved arrow) tibiofibular ligaments. **(b)** Coronal T1-weighted MR image shows the posterior tibiofibular (straight arrow) and posterior talofibular (curved arrow) ligaments. **(3)** Normal talofibular ligaments. Axial T1-weighted MR image depicts the anterior talofibular ligament (arrow). The posterior talofibular ligament normally demonstrates a striated pattern due to interspersed fat (*). Note the oblong shape of the talus as well as the medial indentation of the fibula (*F*), which represents the malleolar fossa. (Reprinted, with permission, from reference 4.)

evaluated on routine orthogonal ankle MR images as long as the section thickness is 3 mm or less.

The anterior and posterior tibiofibular ligaments are usually seen on two or more sequential axial and coronal MR images obtained at the level of the tibial plafond and talar dome (Fig 2). On axial images, these ligaments often appear striated and discontinuous owing to fat interposed between the fascicles of the ligaments and the downward, oblique course of the ligaments toward their insertion on the fibula.

The anterior and posterior talofibular ligaments are usually seen on a single axial image obtained slightly distal to the tibiofibular ligaments. Fluid within the joint serves to highlight the anterior talofibular ligament on T2-weighted images. This ligament appears as a thin, straight, low-signal-intensity band extending from the talus to the fibular malleolus (Fig 3). The posterior talofibular ligament has a fan-shaped insertion on the distal fibula and may demonstrate marked heterogeneity and thickening, which should not be misinterpreted as a tear (Fig 3).

The morphologic features of the talus and the distal fibula can help distinguish the anterior and posterior tibiofibular ligaments from the anterior and posterior talofibular ligaments on axial MR images. The talar dome, where the tibiofibular ligaments are detected, is somewhat square. In addition, the ligaments insert onto the fibula above the malleolar fossa, where the cross-section of the fibula is round. Conversely, the talus is more oblong and the sinus tarsi is partially visualized at the insertion sites of the talofibular ligaments. The fibula demonstrates a medial indentation representing the malleolar fossa.

The calcaneofibular ligament is frequently seen as a band of low signal intensity parallel to the lateral calcaneal wall on routine axial MR images obtained with the foot in plantar flexion

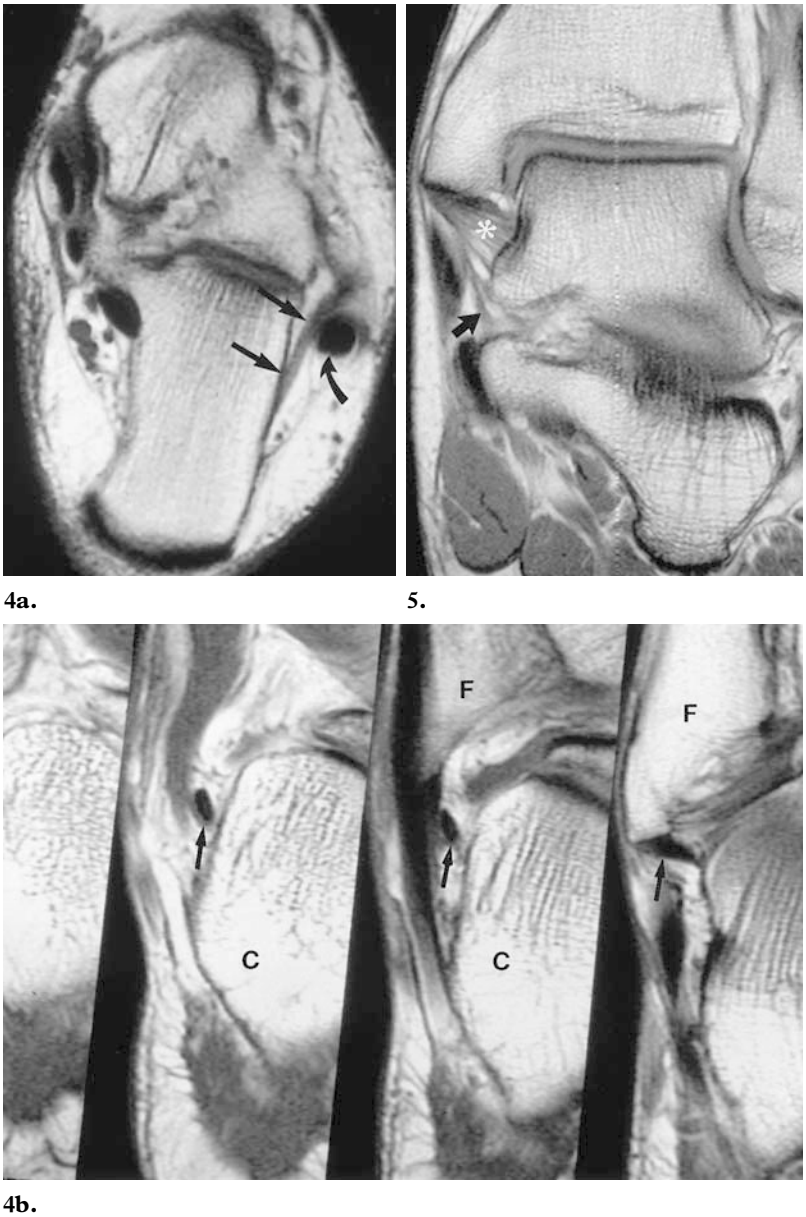

4a. 5.

4b.

Figures 4, 5. **(4)** Normal calcaneofibular ligament. **(a)** Axial T1-weighted MR image shows the calcaneofibular ligament (straight arrows) immediately adjacent to the peroneal tendons (curved arrow). **(b)** Sequential coronal T1-weighted MR images display the calcaneofibular ligament as a round, hypointense structure (arrow) extending from the lateral malleolar tip (*F*) to the lateral wall of the calcaneus (*C*). **(5)** Normal deltoid ligament. Coronal T1-weighted MR image shows the striated posterior tibiotalar (*) and tibiocalcaneal (arrow) bands of the deltoid ligament.

(Fig 4a). However, the ligament is more consistently visualized on coronal images, where it is depicted in cross-section as a round, homogeneous, low-signal-intensity structure that can be followed up on sequential T1-weighted images from its fibular origin to its calcaneal insertion site (Fig 4b). The various components of the deltoid ligament are well visualized on both axial and coronal images. The deep, tibiotalar component of the deltoid ligament normally demonstrates regular striations and thus has a heterogeneous appearance (Fig 5).

Ligamentous Injuries

Lateral ankle sprains represent 16%–21% of all sports-related traumatic lesions. The anterior talofibular ligament is the weakest ligament and therefore the most frequently torn. There is usually a predictable pattern of injury involving the anterior talofibular ligament followed by the calcaneofibular ligament and the posterior talofibular ligament. Anatomic classification of ankle sprains is based on the number of affected ligaments. First-degree sprain is characterized by a partial or complete tear of the anterior talofibular ligament. In second-degree sprain, both the anterior talofibular and calcaneofibular ligaments are either partially or completely torn. Third-degree sprain consists of injuries to the anterior talofibular, calcaneofibular, and posterior talofibular ligaments.

Because acute ankle ligamentous injuries are rarely treated surgically, the use of MR imaging is limited to the evaluation of athletes at advanced competitive levels in whom primary ligamentous surgical repair is contemplated and of

6.

8.

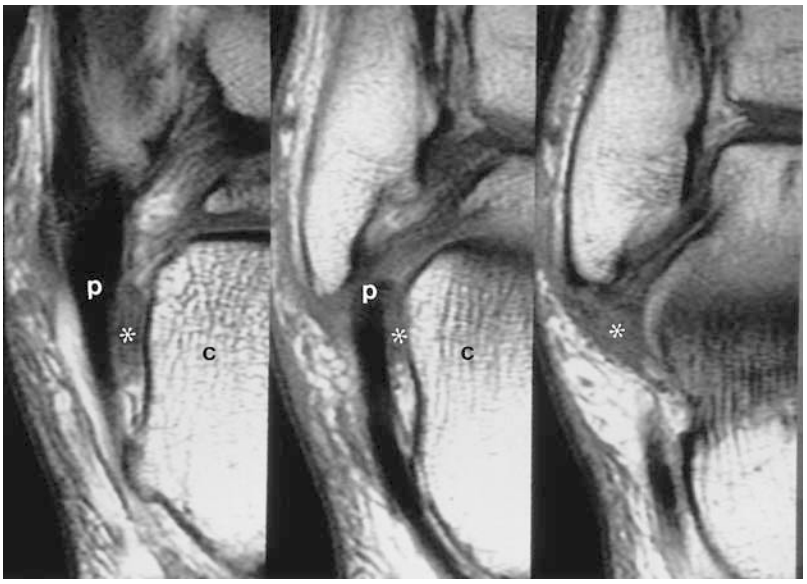

7.

Figures 6–8. **(6)** Chronic tear of the anterior talofibular ligament. Axial T1-weighted MR image demonstrates waviness and irregularity of the anterior talofibular ligament (arrows). **(7)** Injury of the calcaneofibular ligament. Sequential coronal T1-weighted MR images demonstrate increased signal intensity and thickening of the calcaneofibular ligament (*) between the peroneal tendons (*p*) and the lateral wall of the calcaneus (*c*). **(8)** Chronic tear of the calcaneofibular ligament. Axial T2-weighted MR image demonstrates marked thickening and waviness of the calcaneofibular ligament (arrows).

patients with a history of chronic ankle instability (5). The MR imaging criteria for the diagnosis of acute rupture of the lateral collateral ligament include morphologic and signal intensity alterations within and around the ligament (2,6). Injuries of the anterior talofibular ligament are easily seen on routine axial ankle MR images. Discontinuity, detachment, thickening, thinning, or irregularity of the ligament may be encountered. Heterogeneity with increased intraligamentous signal intensity on fat-suppressed or T2-weighted images is indicative of intrasubstance edema or hemorrhage. Obliteration of the fat planes around the ligament, extravasation of joint fluid into the adjacent soft tissues, and talar contusions may also be seen. Chronic tear often manifests as thickening, thinning, elongation, and wavy or irregular contour of the ligament. There is usually no significant residual marrow or soft-tissue edema or hemorrhage (Fig 6). Decreased signal intensity in the fat abutting the ligaments with all pulse sequences is indicative of scarring or synovial proliferation.

Injuries of the calcaneofibular ligament may be detected on routine axial ankle MR images but are more consistently visualized on coronal T1-weighted images (Fig 7). On sequential coronal images, the normal calcaneofibular ligament is seen in cross-section as a low-signal-intensity, homogeneous, oval structure surrounded by fat. The injured ligament is frequently thickened (Fig 8) and heterogeneous, and the surrounding fat planes are often obliterated. Fluid within the peroneal tendon sheath can be a secondary sign of calcaneofibular ligament injury.

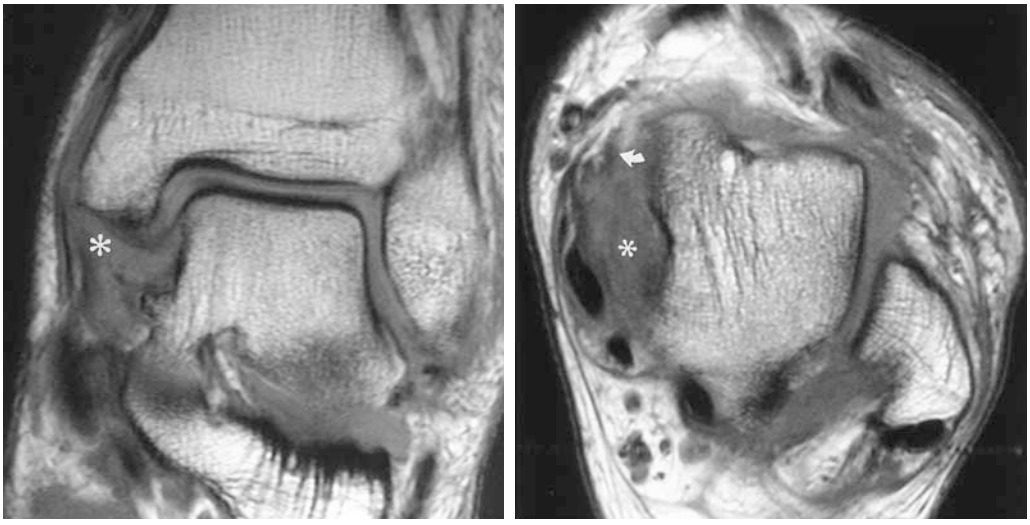

a. **b.**

Figure 9. Injury of the deltoid ligament. Coronal **(a)** and axial **(b)** T1-weighted MR images show indistinctness and swelling of the deltoid ligament as well as loss of the normal pattern of fatty striation (*), findings that are consistent with extensive partial tear. Some fibers of the tibionavicular ligament are still present (arrow in **b**).

MR imaging findings suggest that contusions of the deltoid ligament, particularly of its tibiotalar component, are frequently associated with inversion sprains (7). These contusions manifest as loss of the regular striations that are normally seen in the deltoid ligament (Fig 9). Thus, contrary to what one would expect, the ligament demonstrates homogeneous intermediate signal intensity, a finding that is consistent with injury. Reactive fluid within the tendon sheath of the posterior tibial tendon is also frequently noted.

The accuracy of MR imaging in detecting injuries of the lateral collateral ligament has not yet been clearly established. The accuracy of 3D fast imaging with steady state precision in detecting acute tears of the anterior talofibular and calcaneofibular ligaments is reported to be 94.4% (3). MR arthrography has been shown to have an accuracy of 100% and 82% in detecting chronic anterior talofibular and calcaneofibular ligament tears, respectively, whereas conventional MR imaging has demonstrated an accuracy of 59% in diagnosing chronic lateral collateral ligament tears (8).

Anterolateral Impingement Syndrome

Anterolateral impingement syndrome is a common cause of chronic lateral ankle pain. Injuries to the anterior talofibular and tibiofibular ligaments and an accessory fascicle of the anterior talofibular ligament have been implicated as causes of anterolateral impingement syndrome. Repetitive synovial inflammation secondary to chronic lateral ankle instability produces a soft-tissue "mass" consisting of hypertrophic synovial tissue and fibrosis within the lateral gutter. Anteromedial or anterocentral bone impingement owing to osteophytes at the anterior ankle joint can exacerbate the condition (Fig 10). Arthroscopic debridement of soft-tissue impingement has produced excellent results, with 84% of patients returning to their previous sport activity (9).

MR imaging typically depicts a "meniscoid" mass within the lateral gutter of the ankle that demonstrates low signal intensity with all pulse sequences (Fig 10). This soft-tissue structure is best visualized on axial or coronal images when joint fluid is present within the lateral gutter.

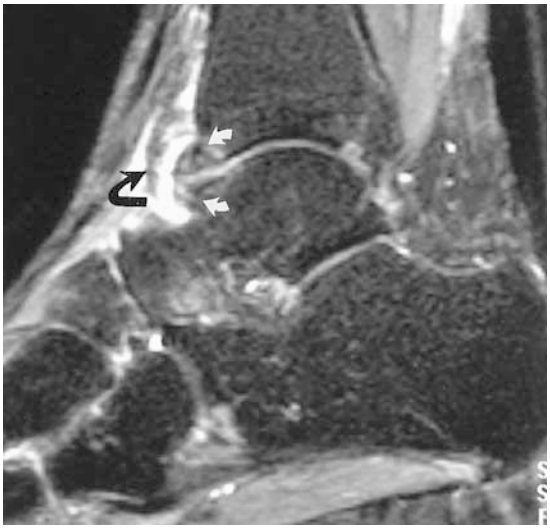

Figure 10. Anterolateral impingement syndrome. Sagittal STIR MR image shows a low-signal-intensity "meniscoid" mass (black arrow) related to redundant synovial tissue. Anterior tibial and talar "kissing" osteophytes are also noted (white arrows).

Figure 11. Sinus tarsi syndrome in a patient with rheumatoid arthritis. Sagittal T1-weighted MR image shows obliteration of fat by an area of fluid-like signal intensity in the subtalar joint (*).

Accurate diagnosis necessitates distinguishing this mass from the adjacent anterior talofibular ligament. The accuracy of routine MR imaging in diagnosing soft-tissue anterolateral impingement syndrome has been questioned, particularly when no joint fluid is present (10–12). MR arthrography may be of value in equivocal cases.

Sinus Tarsi Syndrome

The sinus tarsi is a lateral space located between the talus and the calcaneus. It contains the cervical and interosseous talocalcaneal ligaments, the medial roots of the inferior extensor retinaculum, neurovascular structures, and fat. Sinus tarsi syndrome is caused by hemorrhage or inflammation of the synovial recesses of the sinus tarsi with or without tears of the associated ligaments. This disease entity commonly occurs following an inversion injury and is often associated with tears of the lateral collateral ligaments. It may also be related to rheumatologic disorders and abnormal biomechanics such as flat foot deformity secondary to posterior tibial tendon tear. Patients with sinus tarsi syndrome present with hindfoot instability and pain along the lateral aspect of the foot. Prior to the advent of MR imaging, arthrography of the subtalar joint and relief of pain following injection of a local anesthetic or steroid were the only techniques for diagnosing this syndrome. The MR imaging characteristics of sinus tarsi syndrome include the obliteration of fat in the sinus tarsi space. The space itself is replaced by either fluid or scar tissue, and the ligaments may be disrupted (Fig 11) (13,14). Osteoarthritis of the subtalar joint and subchondral cysts may be present in advanced cases. Normal recesses from the posterior subtalar joint may frequently extend into the sinus tarsi and should not be misinterpreted as pathologic conditions.

Normal Tendon Anatomy

The ankle tendons are well visualized as low-signal-intensity structures with all MR imaging sequences. In general, T1-weighted images provide good anatomic detail, whereas T2-weighted images are useful for assessing the abnormal increase in water that characterizes most pathologic conditions. Axial images are optimal for assessing morphologic features, longitudinal splits, tendon sheath fluid, and adjacent soft-tissue abnormalities. Sagittal images are most useful for depicting disease of the Achilles tendon. Coronal images are the least useful for assessing tendon disease. Occasionally, a minimal amount of fluid is noted within the tendon sheath, but this finding is clinically insignificant. Fluid within the sheath of the flexor hallucis longus tendon is common because of the normal communication between the sheath and the ankle joint.

The magic angle effect produces increased signal within normal tendons when they form an angle of about 55° with the main magnetic vector (15). This phenomenon is usually seen with echo times less than 20 msec (T1-weighted, proton-density–weighted, or gradient-echo sequences) and is quite common in the ankle tendons because they curve around the ankle joint. The posterior tibial tendon is particularly susceptible to the magic angle effect at its insertion on the navicular bone (Fig 12). Striation of the tendon at that site is also due to fat interposed between the several insertional fascicles of the tendon and should not be misinterpreted as a pathologic condition. Imaging the ankle in about 20° of plantar flexion decreases the angle between the tendons and the main magnetic vector and is therefore quite useful in decreasing the magic angle effect.

Figure 12. Magic angle effect in an asymptomatic patient. Axial proton-density–weighted MR image demonstrates increased signal intensity within the posterior tibial (curved arrow), flexor digitorum longus (straight solid arrow), and flexor hallucis longus (open arrow) tendons. (Reprinted, with permission, from reference 16.)

Tendon Injuries

Tendon injuries can be grouped into six categories: tendinosis, peritendinosis, tenosynovitis, entrapment, rupture, and dislocation (17,18). These conditions often coexist, and overlap in their clinical, gross, and histologic manifestations can make them indistinguishable at MR imaging (6). The MR imaging characteristics of tendinosis include a fusiform shape and focal areas of increased tendon girth associated with increased signal intensity within the tendon on T1-weighted and proton-density–weighted images. T2 signal intensity alterations are noted when significant intrasubstance degeneration is present. Tenosynovitis and peritendinosis are caused by inflammation or mechanical irritation of the tendon sheath and peritenon, respectively. MR images reveal fluid accumulation, synovial proliferation, or scarring within the tendon sheath or adjacent soft tissues. Stenosing tenosynovitis occurs when synovial proliferation and fibrosis surround the tendon, causing entrapment and even rupture. It manifests as areas of intermediate to low signal intensity in the soft tissues around the tendon with all MR imaging sequences.

Partial rupture manifests on T1-weighted and proton-density–weighted images and occasionally on T2-weighted images as an area within the substance of the tendon having a signal intensity similar to that seen in advanced tendinosis. Complete rupture is depicted as complete disruption of the tendon fibers. MR imaging is useful in the detection of dislocation and subluxation of the peroneal and posterior tibial tendons and in the assessment of concomitant tendon disease.

13.

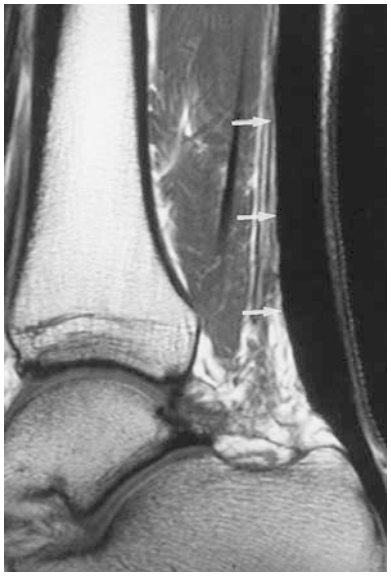

14.

Figures 13, 14. **(13)** Acute Achilles peritendinosis. Sagittal T2-weighted MR image shows a reticular pattern of increased signal intensity in the pre–Achilles tendon fat (*), a finding that indicates the presence of edema. **(14)** Chronic tendinosis of the Achilles tendon. Sagittal T1-weighted MR image shows fusiform thickening of the Achilles tendon without evidence of increased intrasubstance signal intensity (arrows).

Achilles Tendon Injuries

Achilles tendon injuries may be classified as noninsertional or insertional (17,18). The former group includes diffuse acute and chronic peritendinosis, tendinosis, and a rupture 2–6 cm above the insertion of the tendon on the calcaneus (19). The latter group includes insertional Achilles tendinosis, which may be associated with Haglund deformity of the calcaneus. Weinstabi et al (19) classified Achilles tendon lesions into four types on the basis of MR imaging findings. Type I represents inflammatory reaction; type II, degenerative changes; type III, partial rupture; and type IV, complete rupture.

The Achilles tendon lacks a tendon sheath. However, it has a peritenon whose vascular system extends both within and outside the tendon. Achilles peritendinosis manifests at MR imaging as linear or irregular areas of altered signal intensity in the pre–Achilles tendon fat pad, a finding that indicates the presence of edema (Fig 13), or scarring of the peritenon. The tendon itself is normal. Achilles tendinosis manifests on axial MR images as loss of the anterior concave or flat surface of the Achilles tendon and on sagittal images as fusiform thickening of the tendon (Fig 14) (20). Areas of increased signal intensity within the tendon are also noted.

Preoperative MR imaging is useful for distinguishing partial from complete rupture and assessing the site and extent of the tear. Clinical misdiagnosis has been reported in up to 25% of patients with complete tears of the Achilles tendon due to swelling that obscures the tendon gap and retained weak plantar flexion (false-negative Thompson test). At MR imaging, partial Achilles tendon tears demonstrate heterogeneous signal intensity and thickening of the tendon without complete interruption (Fig 15). Differentiation between partial tear and severe chronic Achilles tendinosis may be difficult apart from clinical history. However, acute partial tears are often associated with subcutaneous edema, hemorrhage within the Kager fat pad, and intratendinous hemorrhage at MR imaging, whereas chronic tendinosis does not usually demonstrate increased subcutaneous or intratendinous signal intensity on T2-weighted images. Complete Achilles tendon rupture manifests as discontinuity with fraying and retraction of the torn edges of the tendon (Fig 16). In acute rupture, the tendon gap demonstrates intermediate signal intensity on T1-weighted images and high signal intensity on T2-weighted images, findings that are consistent with edema and hemorrhage, whereas in chronic ruptures, scar or fat

15. 16. 17. 18.

Figures 15–18. **(15)** Partial tear of the Achilles tendon. Sagittal T2-weighted MR image demonstrates a thickened Achilles tendon containing irregular areas of high signal intensity and focal discontinuity of posterior fibers (arrow), findings that are consistent with partial tear. **(16)** Complete tear of the Achilles tendon. Sagittal T2-weighted MR image depicts complete disruption and retraction of the torn edges of the Achilles tendon (arrows) with a fluid-filled gap (*). **(17)** Partial retear of the Achilles tendon following surgical repair in a patient with recurrent symptoms. Sagittal STIR MR image demonstrates thickening and increased signal intensity at the surgical site (arrows) related to retear. Note the punctate and serpentine areas of signal void indicating the presence of surgical material. **(18)** Insertional partial tear of the Achilles tendon. Sagittal STIR MR image shows increased signal intensity at the insertion site of the Achilles tendon (white arrowheads) associated with retrocalcaneal bursitis (black arrowhead). A prominent posterosuperior calcaneal tuberosity (Haglund deformity) and edematous bone marrow (*) are also noted.

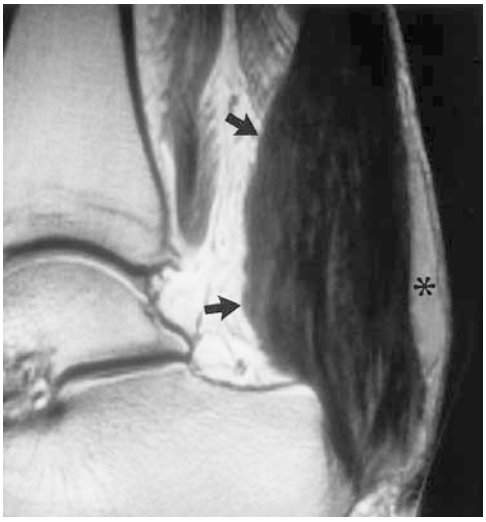

Figure 19. Xanthoma of the Achilles tendon in a patient with familial hypercholesterolemia. Sagittal T1-weighted MR image demonstrates massive enlargement and linear stranding of the Achilles tendon (arrows). Achilles bursitis is also seen (*). (Reprinted, with permission, from reference 4.)

may replace the tendon. Partial rerupture occurs in approximately 2% of surgically treated Achilles tendon ruptures (Fig 17). Postoperative MR imaging assessment includes evaluation of the extent of tendinous union and healing. On most follow-up MR imaging studies, intratendinous signal intensity will decrease as the tendon heals (21). However, the tendon may remain thickened, simulating chronic tendinosis, even after normal signal intensity has been regained.

Insertional tendinosis is frequently associated with Haglund deformity of the calcaneus but may also be related to an ill-fitting shoe or to overuse. Focal pain at the insertion site of the Achilles tendon is usually present at clinical examination. Initial treatment of this condition is conservative. However, surgical treatment with removal of intrasubstance calcifications and bone osteophytes as well as resection of the Haglund deformity has proved highly successful. MR imaging findings include increased signal intensity and thickening at the insertion site of the Achilles tendon, intrasubstance calcifications, Haglund deformity, calcaneal marrow edema, and distended retrocalcaneal and Achilles bursitis (Fig 18).

Fusiform thickening of the Achilles tendon associated with intrasubstance heterogeneity and stippling are consistent with the presence of xanthoma (Fig 19) (22). This entity is usually found in the presence of familial hypercholesterolemia and should be suspected in patients with bilateral Achilles tendon abnormalities. Obviously, differentiation from Achilles tendinosis is important.

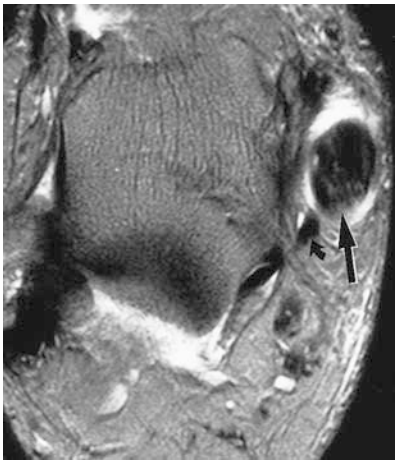

20.

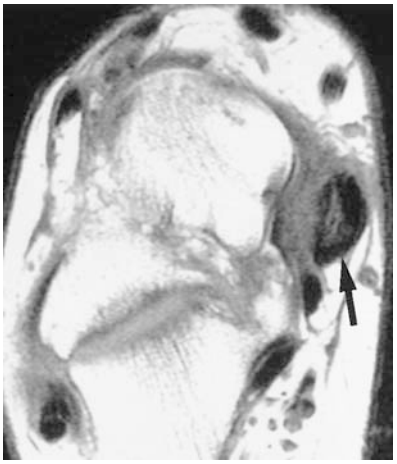

21.

22.

23.

Figures 20–23. **(20)** Type I tear of the posterior tibial tendon. On an axial T2-weighted MR image, the markedly thickened tendon (straight arrow) has a diameter 10 times that of the adjacent flexor digitorum longus tendon (curved arrow). Heterogeneous intrasubstance signal intensity representing longitudinal splits is also noted. **(21)** Advanced type I tear of the posterior tibial tendon. Axial T1-weighted MR image shows marked tendon thickening as well as high-signal-intensity foci (arrow) representing longitudinal splits. **(22)** Type II tear of the posterior tibial tendon. Axial proton-density–weighted MR image shows an attenuated posterior tibial tendon (open arrow) with a caliber equal to that of the adjacent flexor digitorum tendon (solid arrow). **(23)** Type III tear of the posterior tibial tendon. Axial T2-weighted MR image demonstrates absence of the posterior tibial tendon. The tibial retromalleolar groove has been replaced by synovial fluid and debris (arrow). (Reprinted, with permission, from reference 27.)

Posterior Tibial Tendon Dysfunction

Acute or chronic dysfunction of the posterior tibial tendon encompasses a spectrum of abnormalities ranging from tenosynovitis and tendinosis to partial or complete rupture of the tendon. Acute tenosynovitis is related to overuse and is usually encountered in young, athletic individuals. At MR imaging, fluid is seen within the tendon sheath (23). The tendon demonstrates normal signal intensity and morphologic characteristics, although nodular or diffuse thickening in chronic tenosynovitis and scarring of the peritenon may be encountered. Tendinosis manifests as mild to severe heterogeneity and thickening of the tendon.

Chronic posterior tibial tendon rupture typically develops in women during the 5th and 6th decades of life and is associated with progressive flat foot deformity. The tear is commonly noted behind the medial malleolus, where the tendon is subjected to a significant amount of friction. Acute partial or complete rupture of the posterior tibial tendon in young, athletic individuals is less common and is usually seen at the insertion of the tendon on the navicular bone (24).

Surgical and MR imaging classification of chronic posterior tibial tendon ruptures divides these injuries into three types (25). Type I partial tear consists of an incomplete tear with fusiform enlargement, intrasubstance degeneration, and longitudinal splits. On axial MR images, the diameter of the tendon may be five to 10 times that of the adjacent flexor digitorum longus tendon (Fig 20). High-signal-intensity foci representing longitudinal splits are noted within the substance of the tendon on T1-weighted and proton-density–weighted images (Fig 21). Thus, diagnostic overlap exists between severe tendinosis and partial type I tears because both demonstrate fusiform thickening of the tendon with intrasubstance signal intensity alteration (26). Further stretching and elongation of the tendon leads to a type II partial tear of the posterior tibial tendon. On axial images, a decrease in the diameter of the tendon, usually without signal intensity alterations, is diagnostic for this pathologic condition. The caliber of the tendon may now be equal to or less than that of the adjacent flexor digitorum longus tendon (Fig 22). Complete disruption of the tendon fibers is seen in type III posterior tibial tendon tears. These are quite rare and appear at MR imaging as tendon discontinuity. The gap may be filled with fluid or granulation tissue, depending on the chronicity of the injury (Fig 23).

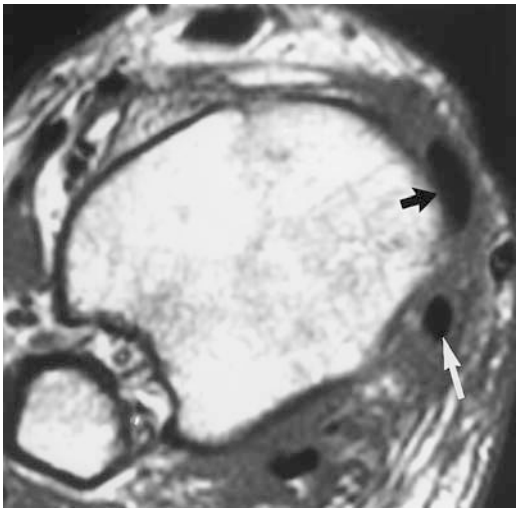

Figure 24. Dislocation of the posterior tibial tendon. Axial proton-density–weighted MR image shows the posterior tibial tendon anterior and medial to the tibial malleolus (black arrow). The flexor digitorum longus tendon is medially displaced within the retromalleolar groove (white arrow). (Reprinted, with permission, from reference 30.)

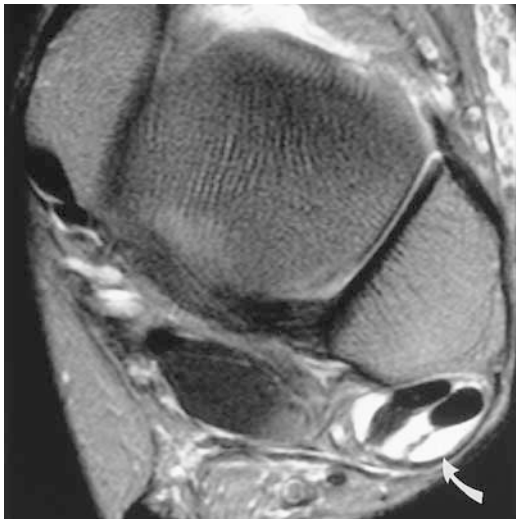

Figure 25. Peroneal tenosynovitis. Axial T2-weighted MR image shows a large amount of fluid within the common peroneal tendon sheath (arrow). The morphologic features of the tendons remain unchanged.

A number of soft-tissue and bone abnormalities are encountered at MR imaging in patients with posterior tibial tendon tears (28). These include fluid within the tendon sheath, fluid within the medial or lateral bursae, sinus tarsi syndrome, periostitis at the insertion of the flexor retinaculum on the tibia, hindfoot valgus, subtalar and talonavicular malalignment, and accessory navicular bone.

Dislocation of the posterior tibial tendon is a rare condition that is most commonly seen in young patients following a recognized injury to the ankle (29). The mechanism of injury is usually related to severe dorsiflexion associated with a torn flexor retinaculum, allowing the tendon to slide out of its groove. On axial MR images, subluxation or complete dislocation of the posterior tibial tendon is easily identified (Fig 24) (30). The tendon is seen medial or anterior to the medial malleolus. Additional findings include an avulsed or stripped flexor retinaculum, pressure erosion of the dislocated tendon on the medial malleolus, and a partially torn tendon.

Peroneal Tendon Injuries

Injuries to the peroneal tendons are frequently encountered and include peritendinosis, tenosynovitis, tendinosis, rupture, and dislocation (31). MR imaging characteristics of peritendinosis and tenosynovitis include scarring around the tendons and fluid within the common tendon sheath, respectively (Fig 25) (32). The morphologic features of the tendon are usually preserved. Care should be taken to differentiate tenosynovitis from fluid within the common peroneal sheath secondary to a tear of the calcaneofibular ligament.

Acute and chronic ruptures of the peroneal tendons occur in young, athletic individuals due to overuse or may be related to degenerative wear and tear in older, more sedentary patients. Calcaneal fractures typically predispose to partial tears, dislocation, and entrapment of the peroneal tendons. Chronic longitudinal tears of the peroneus brevis tendon often originate within the fibular groove, where the tendon is entrapped between the peroneus longus tendon and the lateral malleolus. They may be associated with either superior peroneal retinacular tear or laxity secondary to inversion injury. Longitudinal intrasubstance tears of the peroneus brevis tendon have a distinct appearance on axial MR images (33–35). The tendon assumes a C-shaped or boomerang configuration that partially envelops the peroneus longus tendon (Fig 26). Partial or full substance splits within the tendon and intrasubstance high-signal-intensity foci are noted on both T1- and T2-weighted images.

Acute or chronic tears of the peroneus longus tendon may be associated with peroneus brevis

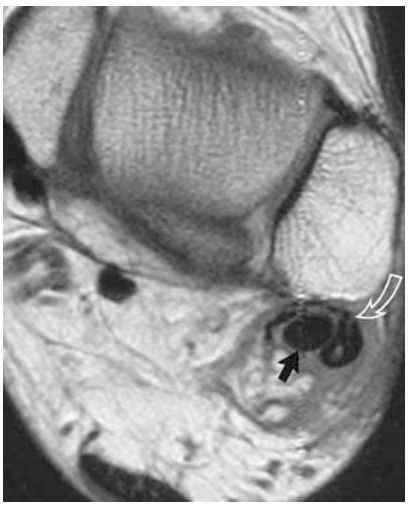

26.

27.

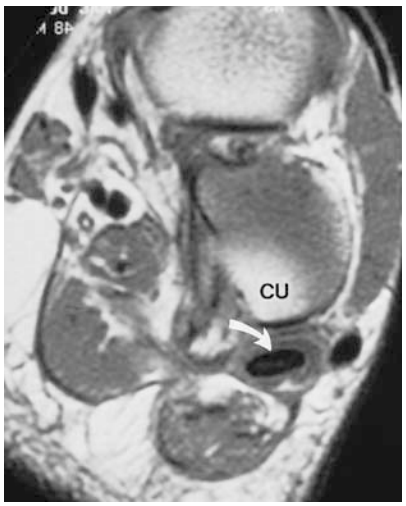

28.

Figures 26–28. **(26)** Longitudinal tear of the peroneus brevis tendon. Axial proton-density–weighted MR image demonstrates a C-shaped split peroneus brevis tendon (white arrow) partially enveloping the peroneus longus tendon (black arrow). **(27)** Partial tear of the peroneus longus and brevis tendons. Axial proton-density–weighted MR image shows splits of the peroneus longus (open arrow) and peroneus brevis (solid white arrow) tendons. Marrow edema (arrowheads) is visible within a prominent peroneal tubercle (*). Debris, fluid, and scar (black arrows) are seen surrounding the tendons. (Reprinted, with permission, from reference 36.) **(28)** Chronic partial tear of the peroneus longus tendon. Oblique coronal T1-weighted MR image reveals increased intrasubstance signal intensity in a thickened peroneus longus tendon (arrow) as it courses inferior to the cuboid bone (*CU*). (Reprinted, with permission, from reference 36.)

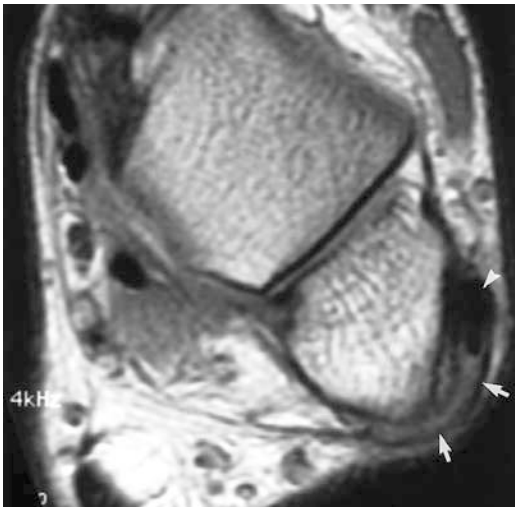

Figure 29. Dislocation of peroneal tendons. Axial proton-density–weighted MR image shows the dislocated peroneus brevis and longus tendons (arrowhead) within a "pouch" formed by the stripped-off superior peroneal retinaculum (arrows).

tendon tears at the level of the medial malleolus (33). Isolated tears of the peroneus longus tendon are more frequently seen at the level of the peroneal tubercle or cuboid tunnel (36) (Figs 27, 28). MR imaging findings include morphologic and signal intensity abnormalities within the tendon representing partial or complete disruption. Marrow edema may be encountered within the lateral calcaneus and within a hypertrophic peroneal tubercle. Occasionally, proximal retraction of the os peroneum may be seen in patients with complete rupture of the peroneus longus tendon.

Dislocation of the peroneal tendons is often clinically misdiagnosed as an ankle sprain. A flake-like fracture of the distal fibular metaphysis may be present on conventional radiographs, indicating an avulsed or stripped peroneal retinaculum. The mechanism of acute dislocation is a violent contraction of the peroneal muscles with secondary detachment of the superior peroneal retinaculum and lateral dislocation of the peroneal tendons out of the retromalleolar groove. Chronic ankle instability associated with superior peroneal retinacular laxity is considered a predisposing factor for chronic peroneal tendon dislocation.

MR imaging allows direct assessment of the position of the tendons relative to the fibular retromalleolar groove (32,34). Dislocation is best demonstrated on axial images, which show the tendons to be located anterior and lateral to the distal fibula. The tendons are often found within a "pouch" formed by a stripped-off superior peroneal retinaculum (Fig 29). Avulsion off the distal fibula and midsubstance tears of the superior

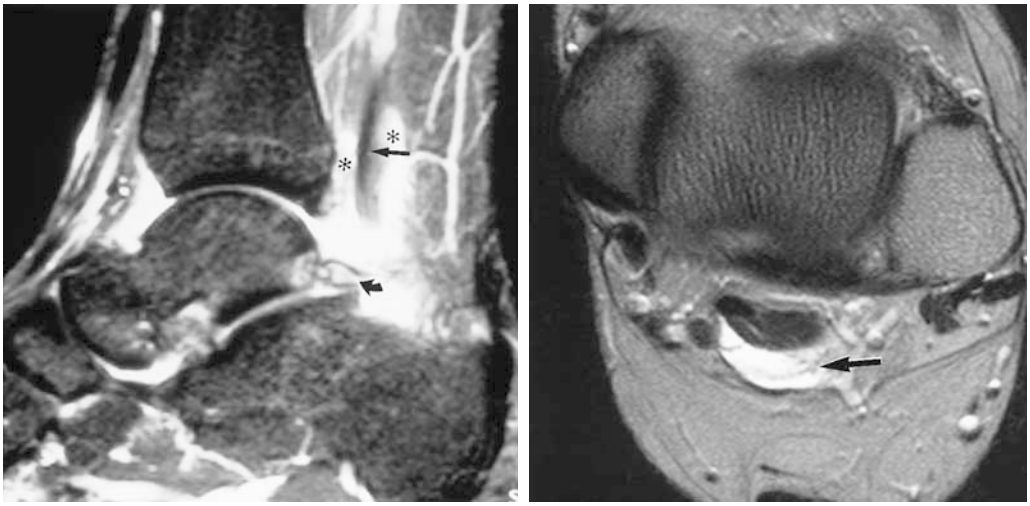

a. b.

Figure 30. Os trigonum syndrome and flexor hallucis longus tenosynovitis. **(a)** Sagittal STIR MR image demonstrates abundant fluid (*) within the sheath of the flexor hallucis longus tendon (straight arrow). Edematous changes of the os trigonum, synchondrosis, and posterior talus (curved arrow) are also seen. **(b)** Axial T2-weighted MR image obtained in a different patient shows fluid and debris within the flexor hallucis longus tendon sheath (arrow), a finding that is consistent with tenosynovitis. Note the absence of joint fluid.

peroneal retinaculum are less frequently encountered. Associated MR imaging findings include tenosynovitis or tears of the peroneal tendons, convex fibular groove, avulsion fracture of the distal fibula, and tear of the lateral collateral ligament.

Flexor Hallucis Longus Tendon Injuries

The flexor hallucis longus tendon is susceptible to injuries as it passes through the fibro-osseous tunnel between the lateral and medial talar tubercles. Repetitive friction at that site predisposes to chronic or stenosing tenosynovitis, tendinosis, and partial tear. Complete tendon rupture may also occur.

Injuries to the flexor hallucis longus tendon are best visualized on axial and sagittal MR images (Fig 30a) (37). Synovial fluid surrounding an otherwise intact tendon is characteristic of chronic tenosynovitis, particularly if only a small amount of fluid is noted within the ankle joint (Fig 30b). Tendon sheath fluid in the presence of a large ankle joint effusion most likely indicates a normal communication between the two structures and is usually of no clinical significance. Chronic and extensive inflammation of the peritenon leads to stenosing tenosynovitis, producing a functional hallux rigidus. Fusiform swelling and longitudinal splitting of the tendon associated with increased intrasubstance signal intensity is indicative of tendinosis and partial tear.

Flexor hallucis longus tenosynovitis and tendinosis may also be seen in the region of the Henry knot and as the tendon passes between the sesamoid bones at the head of the first metatarsal. MR imaging helps distinguish flexor hallucis longus tendon abnormalities from other conditions with similar clinical characteristics (eg, sesamoiditis). Isolated distal rupture of the flexor hallucis longus tendon is a rare condition resulting from acute dorsiflexion or laceration injuries.

Osseous Lesions

Bone Contusion

During the acute stage, bone contusions (bone bruises) manifest at MR imaging as reticular areas of hypointensity on T1-weighted images and hyperintensity on T2-weighted and fat-suppressed images (Fig 31) (38,39). They are related to microfractures of the trabecular bone and edema or hemorrhage within the bone marrow. Bone contusions normally resolve within 8–12 weeks. In most cases, radiographic findings are negative. The clinical significance of bone contusions detected with MR imaging is unknown, but it is generally accepted that continued stress placed on a contused bone may lead to complete fracture (40).

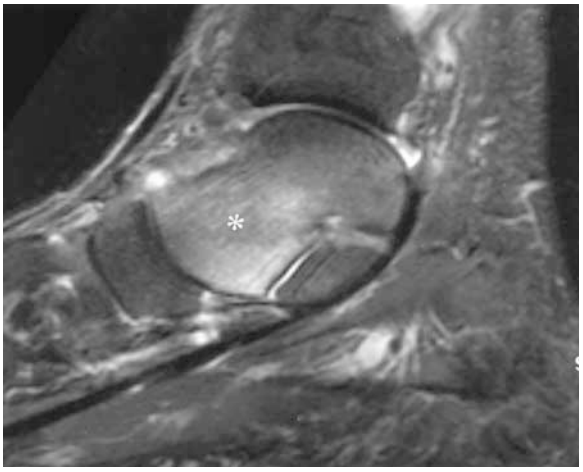

Figure 31. Bone contusion. Sagittal STIR MR image demonstrates increased signal intensity in the anterior talus (*), a finding that is consistent with microtrabecular disruption and edema.

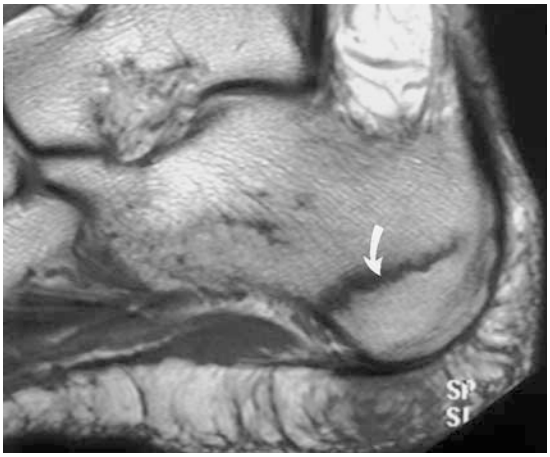

Figure 32. Stress fracture. Sagittal T1-weighted MR image demonstrates a transverse, nondisplaced fracture of the calcaneus (arrow) with surrounding bone marrow edema.

Stress Fractures and Acute Posttraumatic Fractures

Stress fractures and insufficiency fractures occur frequently in the ankle and foot and predominantly involve the second metatarsal, the calcaneus, and, less frequently, the navicular bone and talus (41–44). Prior to stress fracture, a condition known as "stress response" occurs. During this period, edema, hyperemia, and osteoclastic activity develop within the stressed area of the bone, manifesting at MR imaging as poorly defined, abnormal signal intensity of the bone marrow similar to that of a bone contusion with an ill-defined area of hypointensity on T1-weighted images and hyperintensity on T2-weighted images and fat-suppressed images (44,45).

As the stress persists and a fracture develops, MR imaging will show an irregular, hypointense line within the area of edema and hyperemia (Fig 32). Periosteal callus formation begins shortly after the fracture occurs and can be seen at MR imaging as a hypointense line running parallel to the cortex and representing the elevated periosteum. During the first few days, this periosteal reaction may not be seen at conventional radiography because not enough calcium has been deposited. The periosteum is separated from the underlying cortex by hyperintense tissue on T2-weighted images, most likely representing inflammatory reaction (45).

MR imaging has been found to be more sensitive than conventional radiography and more specific than bone scintigraphy in the detection of occult fractures, particularly in the elderly and in osteoporotic patients (46). Acute posttraumatic fractures will appear similar to stress-related fractures at MR imaging, with hypointense lines representing the fracture surrounded by ill-defined areas of edema and hemorrhage.

Osteochondral Fractures

Osteochondral fractures originate from single or multiple traumatic events, leading to partial or complete detachment of an osteochondral fragment with or without associated osteonecrosis. The term *osteochondral lesion* (or *transchondral fracture*) is preferred to the term *osteochondritis dissecans* because it better describes the traumatic nature of these lesions. *Transchondral fracture* refers to those lesions that exclusively involve the articular cartilage with no associated subchondral bone lesion (47).

Osteochondral fractures of the ankle are usually seen in the talar dome, most frequently in the middle third of the lateral border and in the posterior third of the medial border (47). Inversion injuries with dorsiflexion of the foot lead to an osteochondral lesion of the lateral aspect of the talar dome, often associated with a lateral collateral ligament tear. An inversion injury to the ankle with the foot in plantar flexion and lateral rotation of the tibia on the talus lead to a posteromedial talar dome lesion (47,48).

Berndt and Harty (49) have classified osteochondral talar lesions into four stages based on the integrity of the articular cartilage and the condition of the subchondral fragment. Stage I

33.

34.

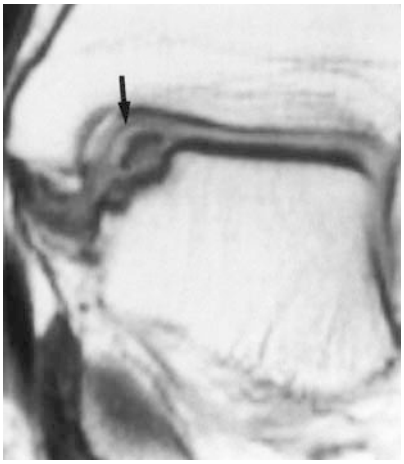

35.

Figures 33–36. **(33)** Stage I osteochondral lesion. Coronal T1-weighted MR image shows a subchondral area of decreased signal intensity in the medial talar dome. **(34)** Stage II osteochondral lesion. Coronal T1-weighted MR image reveals a partially detached osteocartilaginous fragment in the lateral talar dome (arrow). **(35)** Stage III osteochondral lesion. Coronal T1-weighted MR image reveals an osteochondral fragment that is completely detached from the talus (arrow) but is still located within its crater. **(36)** Stage IV osteochondral lesion. Coronal T1-weighted MR image demonstrates a crater in the medial talar dome (white arrow). Note also the separate, nonviable bone fragment displaced away from the donor site (black arrow).

36.

lesions involve the subchondral bone, with preserved integrity of the overlying articular cartilage. Stage II lesions consist of a partially detached fragment of articular cartilage and subchondral bone. Stage III lesions are characterized by a completely detached fragment that is still located within the defect produced by the fracture. Stage IV lesions consist of a completely detached osteochondral fragment located in a joint recess away from the fracture site.

The treatment of osteochondral lesions during the early stages is aimed at revascularization, healing, and prevention of detachment of the fragment. Conservative treatment is recommended when the articular cartilage is preserved and the lesion is considered viable and stable. Surgical treatment with curettage of the lesion and drilling to promote healing is recommended when the lesion appears unstable, when there is articular incongruity, or when the fragment is necrotic (50).

MR imaging is probably the only technique that can provide information regarding the size and location of the lesion, the condition of the overlying articular cartilage, the congruity of the articular surfaces, the viability of the bone fragment, the stability or degree of healing between the osteochondral fragment and the donor site, and the location of the osteochondral fragment if it has become displaced within the joint space (Figs 33–36) (48,51).

The ideal pulse sequence for identifying osteochondral lesions is still a subject of controversy, but recent reports based on knee imaging seem to favor thin-section 3D Fourier transform spoiled gradient-echo techniques with fat saturation (52, 53) and, more recently, fat-saturated fast spin-echo techniques. Some authors have also recommended intraarticular injection of gadolinium-based contrast material for improved visualization of osteochondral lesions (52).

The signal intensity of the interface between normal bone and an osteochondral fragment has received attention in the MR imaging literature

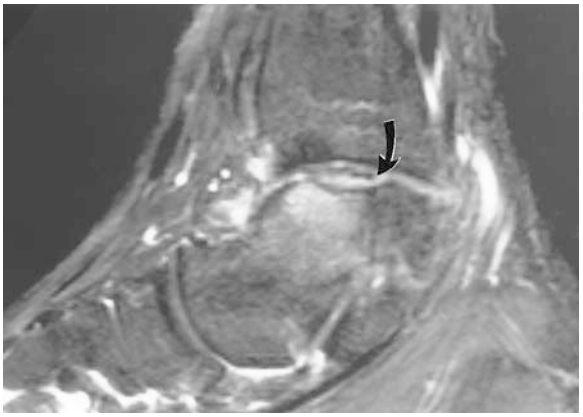

Figure 37. Unstable osteochondral lesion. Sagittal STIR MR image reveals a talar, osteochondral lesion with fluid-like signal intensity interposed between the fragment and the donor site (arrow). Edema of the subchondral talar bone marrow is also seen.

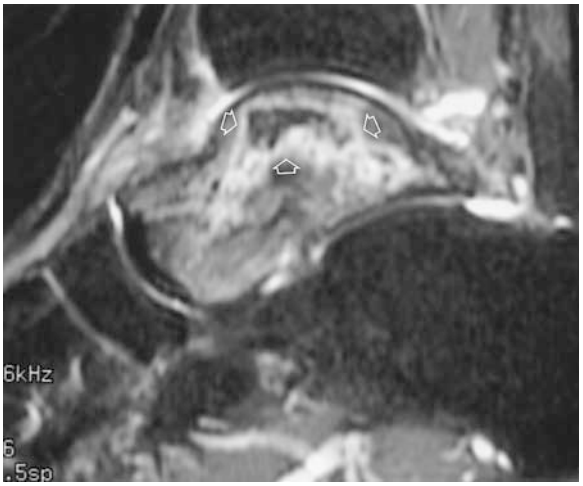

Figure 38. Avascular necrosis of the talus. Sagittal STIR MR image demonstrates serpentine areas of increased signal intensity in the talus (arrows).

(48,51,52). Hypointensity of the interface with T2-weighted pulse sequences indicates healing and stability, whereas hyperintensity may indicate fluid interposed between the fragment and the donor site and, therefore, instability (Fig 37). A potential pitfall is hyperintensity at the interface related to healing granulation tissue. In such cases, intraarticular injection of gadolinium-based contrast material may be helpful. Contrast material interposed between the fragment and the donor site indicates lack of healing and instability. Conversely, if no contrast material is seen at the interface, healing and stability of the fragment with an intact cartilage are expected.

The signal intensity of the fragment itself is also significant. Low signal intensity with all pulse sequences indicates necrosis, whereas hyperintensity on T1-weighted images indicates viable bone marrow (52,53). Viability can be further assessed by means of intravenous injection of gadolinium-based contrast material with fat-suppressed, T1-weighted pulse sequences. Enhancement of the bone marrow of the fragment indicates viable tissue, whereas lack of enhancement indicates nonviable tissue.

Osteonecrosis

Osteonecrosis of the ankle and foot typically occurs in the talus as a consequence of talar neck fractures with vascular compromise of the bone at the level of the sinus tarsi (54). Osteonecrosis of the tarsal navicular bone can occur in children (Kohler disease) and manifests radiographically as sclerosis, irregularity, and fragmentation of the bone. A form of osteonecrosis of the tarsal navicular bone has also been described in adults (Mueller-Weiss syndrome). It occurs more frequently in women and is often bilateral. Deformity and collapse begin in the lateral aspect of the navicular bone and assume a comma-like shape with subsequent superior protrusion of the fragments (55).

Osteonecrosis of the ankle and foot region is also frequently seen in the second metatarsal head (Freiberg disease), with sclerosis and flattening of the metatarsal head seen at conventional radiography, and in the first metatarsal sesamoid bone (54). MR imaging is valuable in assessing the presence, size, and fragment viability of posttraumatic osteonecrosis. Areas of inhomogeneous signal intensity surrounded by a hypointense band, sometimes with a second band of high signal intensity on T2-weighted images (double line sign), are characteristic findings in osteonecrosis of the femoral head before subchondral fracture and collapse occur (56). These findings can also be seen in posttraumatic osteonecrosis of the talus (Fig 38).

Osteonecrosis involving the head of the second metatarsal, tarsal navicular, or sesamoid bone exhibits MR imaging features somewhat different

Figure 39. Freiberg disease. Oblique axial T2-weighted MR image of the foot demonstrates a focus of decreased signal intensity in the head of the second metatarsal (arrow). (Reprinted, with permission, from reference 4.)

Figure 40. Tarsal tunnel syndrome secondary to ganglion cyst. Axial T2-weighted MR image reveals a ganglion cyst (*) interposed between the flexor digitorum longus (*d*) and flexor hallucis longus (*h*) tendons and abutting the adjacent neurovascular bundle (arrow).

from those described in osteonecrosis of the talus. Low signal intensity without an obvious demarcating interface is seen on both T1- and T2-weighted images (Fig 39).

Transient Bone Marrow Edema

Transient bone marrow edema is usually seen in the femoral head and neck (transient osteoporosis of the hip) but can also involve the tarsal bones as part of the syndrome of transient migratory osteoporosis (57). Only anecdotal cases of this entity involving the tarsal bones have been described at MR imaging, which demonstrated changes compatible with bone marrow edema, with ill-defined areas of low signal intensity on T1-weighted images and high signal intensity on T2-weighted images.

Compressive Neuropathies

The most common compressive neuropathies of the ankle and foot are tarsal tunnel syndrome and Morton neuroma. Less frequently seen compressive neuropathies include deep and superficial peroneal nerve entrapment syndromes and sural nerve entrapment syndrome.

Tarsal Tunnel Syndrome

Tarsal tunnel syndrome is characterized by pain and paresthesia in the plantar aspect of the foot and toes (58). This syndrome is most frequently unilateral, as opposed to carpal tunnel syndrome, which is typically bilateral. Nerve entrapment or compression can occur at the level of the posterior tibial nerve or its branches (medial calcaneal nerve, lateral plantar nerve, medial plantar nerve), producing different symptoms depending on the site of compression (Fig 40) (58). Intrinsic and extrinsic causes of posterior tibial nerve compression have been identified. Intrinsic lesions that often produce tarsal tunnel syndrome include accessory muscles, ganglion cysts, neurogenic tumors, varicose veins, lipomas, synovial hypertrophy, and scar tissue. Foot deformities, hypertrophic and accessory muscles, accessory ossicle (os trigonum), and excessive pronation during participation in some sports are just a few of the extrinsic causes of this syndrome (58). In about 50% of cases, the cause of tarsal tunnel syndrome cannot be identified. Relief of symptoms following retinacular release is frequently seen in these idiopathic cases.

At clinical examination, patients present with insidious onset of pain, paresthesia, and a tingling or burning sensation as well as positive Tinnel sign along the plantar and medial aspects of the foot and great toe. The heel is often spared. Pain is exacerbated with exercise, possibly due to venous engorgement. Electromyographic findings are positive in most cases, but in the early stages of the disease they may be falsely negative (58).

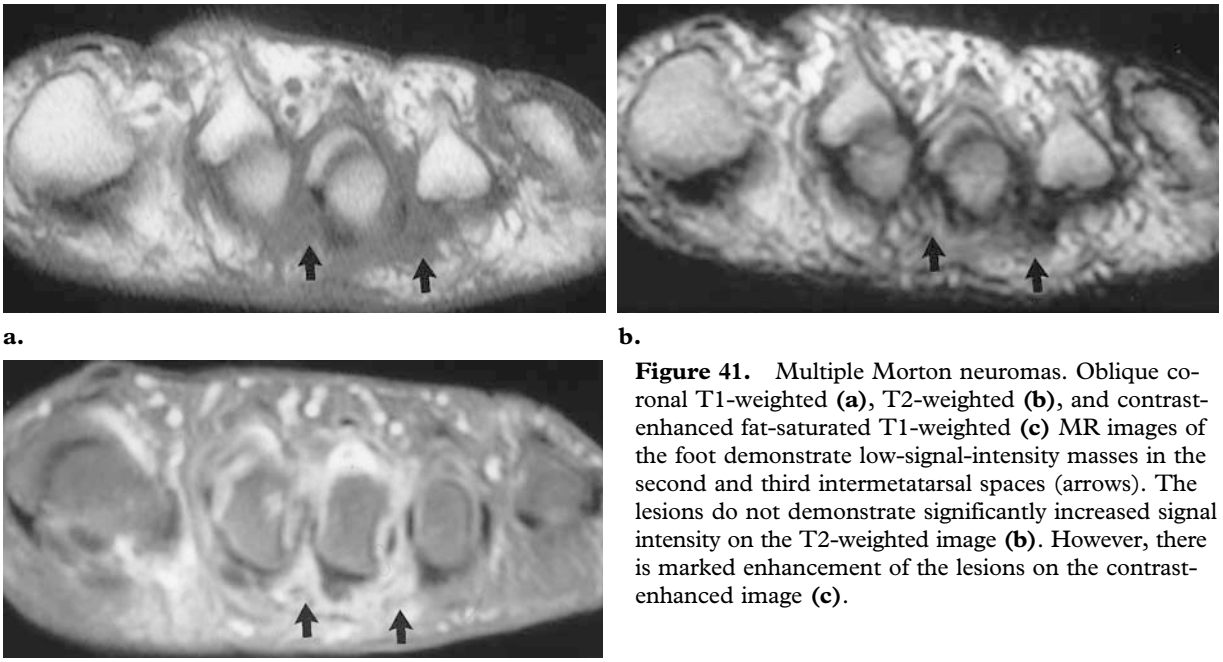

a. **b.** **c.**

Figure 41. Multiple Morton neuromas. Oblique coronal T1-weighted **(a)**, T2-weighted **(b)**, and contrast-enhanced fat-saturated T1-weighted **(c)** MR images of the foot demonstrate low-signal-intensity masses in the second and third intermetatarsal spaces (arrows). The lesions do not demonstrate significantly increased signal intensity on the T2-weighted image **(b)**. However, there is marked enhancement of the lesions on the contrast-enhanced image **(c)**.

MR imaging has been shown to be useful in the preoperative assessment of mass-occupying lesions within the tarsal tunnel.

Morton Neuroma

Morton neuroma (interdigital neuroma) is actually a fibrosing degenerative process produced by compression of a plantar digital nerve. The condition has a female predilection and is frequently seen between the heads of the third and fourth metatarsals, although all web spaces may be involved. The nerve becomes thickened, and associated bursitis is often present. Exquisite tenderness is elicited on lateral compression of the metatarsals. The pain can radiate to the toes and may be accompanied by numbness (59).

Radiographic evaluation of the foot is generally not helpful. However, MR imaging has proved highly accurate in the diagnosis of Morton neuroma, which manifests as a dumbbell-shaped mass located between the metatarsal heads and having intermediate to low signal intensity on both T1- and T2-weighted images (Fig 41). T1-weighted sequences are probably more helpful because the hypointense neuroma is made more conspicuous by the surrounding hyperintense fat. The low signal intensity of Morton neuroma is attributed to the presence of fibrous tissue. Mild enhancement following intravenous injection of gadolinium-based contrast material has been described in some cases (60). A homogeneously hyperintense mass seen between the metatarsal heads without plantar extension on a T2-weighted image usually represents an intermetatarsal bursa and should not be confused with a neuroma.

Synovial Disorders

Pigmented Villonodular Synovitis

Pigmented villonodular synovitis (PVNS) is characterized by inflammatory proliferation of the synovium associated with deposits of hemosiderin. It can be present in any joint, tendon sheath, or bursa but is most frequently seen in the knee, hip, ankle, and elbow. When it originates in the tendon sheaths, the term *giant cell tumor of the tendon sheaths* is often used. In the foot, this lesion predominantly involves the peroneal and flexor tendon sheaths (61).

PVNS can occur at age 20–50 years and may manifest as a focal mass or as a generalized lesion involving the entire joint space. Pressure erosions may be present in the diffuse form. These lesions manifest clinically as joint pain and swelling of long duration, and most are slowly progressive. At pathologic analysis, PVNS is characterized by synovial inflammation with giant cell proliferation, collagen, and lipid-laden macrophages. Treatment of PVNS often consists of resection of the lesion. However, a recurrence rate of 10%–20% is reported in the focal forms and of up to 50% in the diffuse forms (61).

PVNS has characteristic MR imaging features due to the paramagnetic effect of hemosiderin, which produces focal areas of hypointensity with all pulse sequences, mixed with hypointense areas on T1-weighted images and hyperintense areas on T2-weighted images (Fig 42) (61,62). The short T2 relaxation times produced by hemosiderin in the tissues is better observed with high-field-strength magnets. Occasionally, hyperintense areas may be seen within the lesion on T1-weighted images owing to the presence of fat or synovial hemorrhage. Occasionally, a low-signal-intensity rim is seen surrounding the lesion. Joint effusion is often present, producing hypointense areas on T1-weighted images and hyperintense areas on T2-weighted images.

Figure 42. PVNS. Sagittal T1-weighted MR image reveals multiple low-signal-intensity nodules within the tibiotalar joint (arrows) associated with articular surface erosion of both bones. (Reprinted, with permission, from reference 4.)

Soft-Tissue Ganglion Cysts

Ganglion cysts are unilocular or multilocular cysts consisting of mucoid material surrounded by a fibrous capsule. Ganglion cysts may communicate with an adjacent joint or tendon sheath but may also be a completely separate lesion. The most frequent location is the wrist, followed by the ankle and knee. In the ankle and foot, ganglion cysts are seen most frequently in the dorsal aspect or in the region of the sinus tarsi, where they can compress the posterior tibial nerve (see Tarsal Tunnel Syndrome). Ganglion cysts typically occur in the 2nd to 4th decades of life and manifest clinically as focal masses producing dull pain or limited motion. Treatment consists of complete excision of the ganglion cyst to prevent local recurrence (63).

MR imaging is being used extensively to evaluate painful conditions of the ankle and foot, and it is not unusual to find ganglion cysts when imaging a patient for nonspecific pain. Regardless of anatomic location, ganglion cysts manifest at MR imaging as homogeneously hypointense masses on T1-weighted images and hyperintense masses on T2-weighted images (Fig 40). Normally, they are rather well demarcated by their fibrous capsule, and their "tail" or extension into an adjacent joint or tendon sheath (if present) is usually well demonstrated at MR imaging due to the multiplanar capabilities of this modality (63). Lack of enhancement following intravenous administration of gadolinium-based contrast material aids in distinguishing ganglion cysts from solid masses.

Inflammatory Arthritis

MR imaging has been used to evaluate patients with different types of inflammatory arthritis and can demonstrate abnormalities in the bones and soft tissues before they become evident at conventional radiography (Fig 43) (64). This is made possible by the multiplanar capabilities of MR imaging and its exquisite soft-tissue contrast resolution, which allows early detection of bone erosions and very small amounts of fluid in the tendon sheaths, joints, and bursae as well as visualization of pannus formation. Pannus is largely composed of fibrous tissue, but at unenhanced MR imaging it may have signal intensity characteristics similar to those of joint fluid. Therefore, gadolinium-enhanced imaging has been recommended to determine the amount of pannus existing in a joint and to assess the response to therapy (65). Following intravenous injection of contrast material, the normally hypervascular pannus becomes hyperintense on T1-weighted images while the adjacent joint fluid remains hypointense. Delayed enhancement of the joint fluid due to diffusion of the contrast material from the synovium to the joint space has been described; therefore, it is recommended that imaging be performed shortly after injection (65).

Chronic pannus may be accompanied by hemosiderin deposition due to repeated episodes of

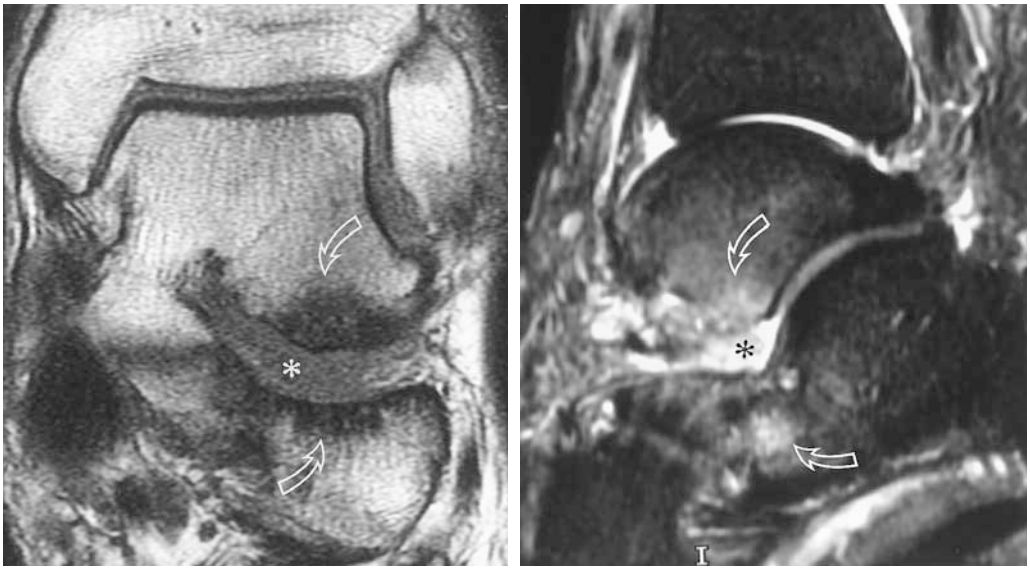

a. b.

Figure 43. Rheumatoid arthritis. Coronal T1-weighted **(a)** and sagittal STIR **(b)** MR images show fluid and debris filling the sinus tarsi (*) as well as cysts and subchondral edema (arrows).

bleeding. It is identified at MR imaging by virtue of the paramagnetic effect of hemosiderin, which produces focal areas of hypointensity with T1- and T2-weighted pulse sequences. The use of heavily T2-weighted pulse sequences with repetition times over 2,000 msec and echo times between 110 and 130 msec has been recommended to identify pannus without having to inject gadolinium-based contrast material.

In patients with inflammatory arthritis, MR imaging can also be used to better depict ruptures of the ligaments and tendons, bursitis, and articular cartilage thinning as well as other less common abnormalities such as rheumatoid nodules, plantar fasciitis, and gouty tophi. In the region of the ankle and foot, the changes of inflammatory arthritis occur most frequently in the metatarsophalangeal and subtalar joints. Synovial proliferation in the region of the sinus tarsi may produce sinus tarsi syndrome. During the acute phase of inflammatory arthritis, signal intensity abnormalities similar to those seen in bone marrow edema may be encountered. This is probably related to hyperemia of the bone marrow adjacent to an acutely inflamed joint (65).

Early articular cartilage erosions in inflammatory arthritis may be difficult to identify with conventional MR imaging sequences (eg, T1- and T2-weighted sequences) because joint fluid may have signal intensity characteristics similar to those of adjacent cartilage. The erosion may also be too small to be seen with 3–5-mm thick sections. In such cases, it is recommended that specialized sequences (eg, 3D gradient-echo T1-weighted sequences, fat-suppressed sequences) that allow excellent depiction of articular cartilage abnormalities be used.

Rheumatoid nodules may be seen in the feet of patients with long-standing rheumatoid arthritis and manifest clinically as painful soft-tissue masses. At MR imaging, rheumatoid nodules have a heterogeneous appearance with irregular margins, probably indicating the presence of surrounding fibrosis, and manifest as focal areas of hyperintensity on T2-weighted images.

Crystal Deposition Disease

The MR imaging manifestations of gout include bone erosion, inflammatory changes of the joint (periarticular edema, bone marrow edema, joint effusion, cartilage thinning, thickened synovium),

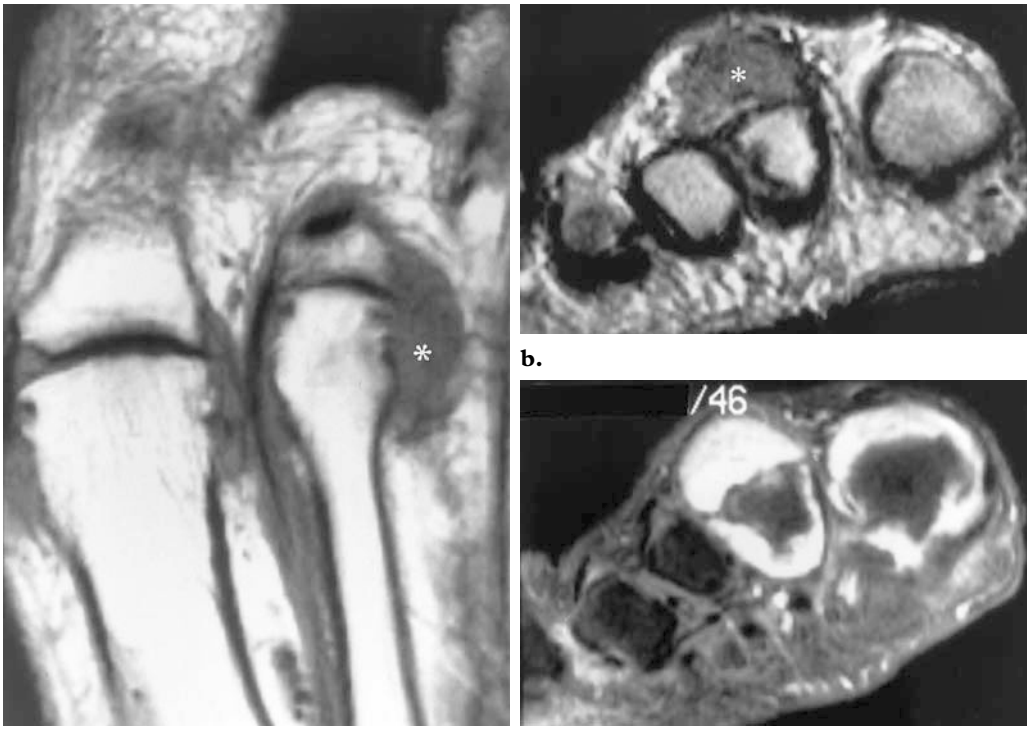

Figure 44. Gout. Long-axis T1-weighted **(a)**, short-axis T2-weighted **(b)**, and contrast-enhanced fat-saturated T1-weighted **(c)** MR images demonstrate a tophus adjacent to the second metatarsophalangeal joint (*) with low signal intensity on **a** and **b** and high signal intensity on **c**. Note the presence of a second enhancing tophus in the first metatarsophalangeal joint in **c**. (Reprinted, with permission, from reference 4.)

and articular or periarticular nodules (tophi) (Fig 44). Lesions are particularly common in the first metatarsophalangeal joint. Gouty tophi are characteristically hypointense with T1- and T2-weighted pulse sequences, perhaps due to their fibrous composition and the presence of urate crystals.

Hemophilic Arthropathy

Patients with hemophilia may develop severe, disabling arthropathy with secondary foot deformities such as talipes equinus, varus, or cavus due to repeated episodes of hemarthrosis. The ankle is the most frequently affected joint, usually during the 2nd decade of life (66). Because of hemosiderin deposition in the hypertrophic synovium, MR imaging will demonstrate intraarticular areas of signal loss in association with other signs of arthritis such as joint space narrowing, cysts, erosions, and sclerosis (Fig 45) (66). These findings are not specific and may also be seen in PVNS, but in the proper clinical setting they suggest hemophilic arthropathy. In severe cases, MR imaging assessment of the degree of synovial hypertrophy can be used to plan synovectomy. In addition to PVNS and hemophilic arthropathy, other joint conditions that may demonstrate intraarticular areas of hypointensity on T1- and T2-weighted images include rheumatoid arthritis, intraarticular hemangioma, gout, and amyloid arthropathy.

Miscellaneous Conditions

Diabetic Foot

MR imaging has been shown to be highly sensitive in the detection and staging of a number of musculoskeletal infections including cellulitis,

Figure 45. Hemophiliac arthropathy. Sagittal T1-weighted MR image shows low-signal-intensity areas anterior and posterior to the tibiotalar joint (*) representing hemosiderin deposition in the hypertrophic synovium due to repeated episodes of hemarthrosis. Note the similarity of these findings with those seen in PVNS (cf Fig 42). (Reprinted, with permission, from reference 4.)

Figure 46. Surgically proved osteomyelitis following penetrating trauma. Sagittal STIR MR image reveals markedly increased signal intensity of the fifth metatarsal head and proximal phalanx (*) with mild joint effusion.

soft-tissue abscesses, and osteomyelitis. MR imaging has greater specificity and better spatial resolution than bone scintigraphy and also has the capacity to provide a quicker diagnosis (67–70).

The MR imaging manifestations of diabetic foot depend on the type of lesion. Acute osteomyelitis demonstrates hypointensity of the bone marrow on T1-weighted images and increased signal intensity on T2-weighted and STIR images (Fig 46). In most patients with diabetic foot, the onset of osteomyelitis is relatively acute, and the signs of subacute or chronic osteomyelitis (Brodie abscess, sequestra formation, cloacae) may not be present.

Periostitis is frequently seen in acute osteomyelitis and can be identified at conventional radiography in patients with either osteomyelitis or neuroarthropathy. MR imaging is highly sensitive in the detection of periostitis, and some reports indicate that it may be more sensitive than conventional radiography in this setting. This is probably because the periosteum is hypocellular and is composed mainly of fibrous tissue that is hypointense with all pulse sequences. The low-signal-intensity periosteum is delineated by the hyperintense inflammatory infiltrate that separates it from the cortical bone and the adjacent soft tissues. The MR imaging appearance of multiple tissue layers each demonstrating different signal intensity characteristics produces rather typical findings in the oblique coronal planes (Fig 47) (68–70). All of these findings can be observed very early in acute osteomyelitis, probably within hours of the onset of infection. In contrast, this disease entity may take anywhere from a few days to 2 weeks to appear on conventional radiographs because of the delay in the radiographic appearance of calcification.

The MR imaging manifestations of soft-tissue infection also depend on the type of infection. Soft-tissue abscesses, which are common in patients with diabetic foot, demonstrate fluid-like signal intensity surrounded by a hypointense rim,

Figures 47–49. **(47)** Diabetic foot in a patient who had undergone transmetatarsal amputation of the first metatarsal. Long-axis T1-weighted MR image reveals recurrent osteomyelitis of the first metatarsal stump, decreased signal intensity within the bone marrow, periostitis (small straight arrows), and surrounding abscess (curved arrow). Note also the presence of septic arthritis and osteomyelitis with bone destruction and periostitis of the second metatarsophalangeal joint (large straight arrow). **(48)** Infected tenosynovitis in a diabetic foot. Oblique axial T2-weighted MR image demonstrates fluid-distended synovial sheaths of the extensor digitorum and peroneal tendons (arrows). **(49)** Neuroarthropathy in a diabetic foot. **(a)** Long-axis T1-weighted MR image shows decreased signal intensity of the tarsal and proximal metatarsal bones. **(b)** Sagittal T2-weighted MR image demonstrates midfoot collapse and low signal intensity of the bone marrow. Osteomyelitis would produce bone marrow edema with a hyperintense appearance on T2-weighted images. (Figures 47–49 reprinted, with permission, from reference 4.)

47.

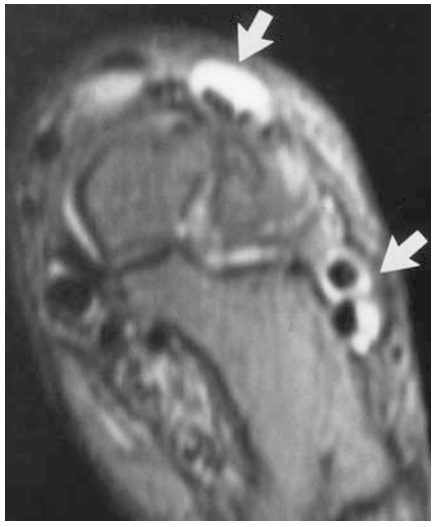

48.

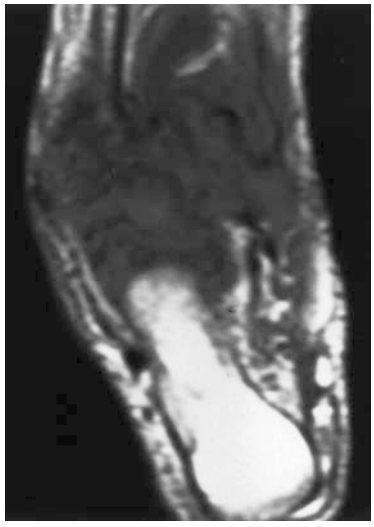

49a.

49b.

which presumably represents the capsule of the abscess. This capsule may be quite thick in chronic abscesses. Sometimes, areas of low signal intensity are seen within the abscess, probably representing cellular debris. In contrast, cellulitis demonstrates nonencapsulated abnormal signal intensity that diffusely infiltrates the subcutaneous tissues and occasionally extends into the deep fasciae (68–70). Synovitis involving the tendons and joints of the ankle and foot is frequently seen in diabetic patients. Fluid-like material is seen distending the tendon sheaths or within the joints (Fig 48). This finding is important because distal infection of the foot may extend proximally above the ankle joint through the tendon sheaths. In such cases, proximal images should be obtained to properly assess the extent of infection, especially if amputation is contemplated.

Differentiation between neuroarthropathy and infection may be difficult with any imaging technique (71). At MR imaging, neuroarthropathy exhibits characteristic findings including bone fragmentation, dislocations, cortical and periosteal thickening, joint effusion, and soft-tissue swelling. In most cases, the bone marrow appears hypointense on both T1- and T2-weighted images (Fig 49). In osteomyelitis, on the other hand, the bone marrow appears hypointense on T1-weighted images and hyperintense on T2-weighted images. In some circumstances, however, the bone

Figure 50. Tear of the plantar fascia. Sagittal T2*-weighted gradient-echo MR image demonstrates discontinuity and intrasubstance tearing at the calcaneal insertion site of the plantar fascia (arrow). Note also the edematous subcutaneous tissue (*).

marrow changes in neuroarthropathy and osteomyelitis are similar, making differentiation between the two entities difficult (71).

Intravenous injection of gadolinium-based contrast material can be used to increase the diagnostic accuracy of MR imaging in soft-tissue and bone infections. Soft-tissue abscesses are often more conspicuous after contrast material injection. Bone marrow enhancement is usually indicative of osteomyelitis, although one should keep in mind that enhancement of noninfected bone marrow edema may occasionally occur. In some cases, the use of fat-suppressed T2-weighted sequences can obviate intravenous injection of gadolinium-based agents (72).

Plantar Fasciitis

Plantar fasciitis is most likely related to repetitive trauma and mechanical stress, which produce microtears and inflammation of the fascia and perifascial soft tissues. Plantar fasciitis is common in runners and obese patients (73,74). Inflammation of the plantar fascia can produce heel pain even in the absence of a traumatic event (73). Patients with plantar fasciitis present with pain at the origin of the plantar fascia. The pain is exacerbated by dorsiflexion of the toes and is more severe in the morning.

Lateral radiographs obtained in patients with plantar fasciitis often demonstrate calcaneal spurs. However, this finding is not specific because it can be seen in about 25% of the asymptomatic population. Bone scintigraphy may demonstrate increased radiotracer uptake in the region of the calcaneus, probably representing periosteal inflammation (73). MR imaging is useful in distinguishing plantar fasciitis from other causes of heel pain and in excluding plantar fascia tears (73,74). On sagittal and coronal MR images, the normal plantar fascia appears as a thin, hypointense structure extending anteriorly from the calcaneal tuberosity. The plantar fascia has a normal thickness of 3.22 mm ± 0.53 and flares slightly at the calcaneal insertion. When inflammatory changes take place, it becomes thickened (up to 7–8 mm) and demonstrates intermediate signal intensity on T1-weighted and proton-density–weighted images and hyperintensity on T2-weighted images (Fig 50). These changes are most prominent in the proximal portion of the plantar fascia at or near its insertion on the calcaneus. Signal intensity changes may also be present in the subcutaneous fat, in the deep soft tissues, and in the calcaneus near the fascial insertion. Thickening is often fusiform, in contrast with plantar fibromatosis, which demonstrates focal, nodular thickening. Discontinuity of the fibers of the plantar fascia, often with focal edema and hemorrhage, is noted when a tear of the fascia is present. Treatment of plantar fasciitis is initially conservative and includes orthotic therapy and administration of nonsteroidal antiinflammatory agents. In more severe cases, local injection of steroids or resection of the fascia may be required. Persistent thickening of the plantar fascia with morphologic and signal intensity alterations at the entheses have been noted in asymptomatic volunteers following fasciotomy (75).

Conclusions

MR imaging is the modality of choice for optimal detection of most soft-tissue disorders of the tendons, ligaments, and other soft-tissue structures of the ankle and foot. This modality is also invaluable in the early detection and assessment of a variety of osseous abnormalities seen in this anatomic location.

References

1. Muhle C, Frank LR, Rand T, et al. Collateral ligaments of the ankle: high-resolution MR imaging with a local gradient coil and anatomic correlation in cadavers. RadioGraphics 1999; 19:673–683.
2. Mesgarzadeh M, Schneck CD, Tehranzadeh J, Chandnani VP, Bonakdarpour A. Magnetic resonance imaging of the ankle ligaments: emphasis on anatomy and injuries to lateral collateral ligaments. Magn Reson Imaging Clin N Am 1994; 2:39–58.
3. Verhaven EF, Shahabpour M, Handelberg FW, Vaes PH, Opdecam PH. The accuracy of three-dimensional magnetic resonance imaging in the diagnosis of ruptures of the lateral ligaments of the ankle. Am J Sports Med 1991; 19:583–587.
4. Beltran J, Rosenberg ZS. Ankle and foot. In: Stark DD, Bradley WG, eds. Magnetic resonance imaging. 3rd ed. St Louis, Mo: Mosby–Year Book, 1999; 873–929.
5. Kannus P, Renstrom P. Treatment for acute tears of the lateral ligaments of the ankle. J Bone Joint Surg [Am] 1991; 73:305–312.
6. Bencardino J, Rosenberg ZS, Delfaut E. MR imaging of sports injuries of the foot and ankle. Magn Reson Imaging Clin N Am 1999; 7:131–149.
7. Klein MA. MR imaging of the ankle: normal and abnormal findings in the medial collateral ligament. AJR Am J Roentgenol 1994; 162:377–383.
8. Chandnani VP, Harper MT, Ficke JR, et al. Chronic ankle instability: evaluation with MR arthrography, MR imaging, and stress radiography. Radiology 1994; 192:189–194.
9. Liu SH, Raskin A, Osti L, et al. Arthroscopic treatment of anterolateral ankle impingement. Arthroscopy 1994; 10:215–218.
10. Rubin DA, Tishkoff NW, Britton CA, Conti SF, Towers JD. Anterolateral soft-tissue impingement in the ankle: diagnosis using MR imaging. AJR Am J Roentgenol 1997; 169:829–835.
11. Farooki S, Yao L, Seeger LI. Anterolateral impingement of the ankle: effectiveness of MR imaging. Radiology 1998; 207:357–360.
12. Jordan LK, Helms CA, Cooperman AE, Speer KP. Magnetic resonance imaging findings in anterolateral impingement of the ankle. Skeletal Radiol 2000; 29:34–39.
13. Klein MA, Spreitzer AM. MR imaging of the tarsal sinus and canal: normal anatomy, pathologic findings and features of the sinus tarsi syndrome. Radiology 1993; 185:233–240.
14. Beltran J. Sinus tarsi syndrome. Magn Reson Imaging Clin N Am 1994; 2:59–65.
15. Erickson SJ, Cox IH, Hyde JS, Carrera GF, Strandt JA, Estkowski LD. Effect of tendon orientation on MR imaging signal intensity: a manifestation of the "magic angle" phenomenon. Radiology 1991; 181:389–392.
16. Rosenberg ZS, Mellado J, Bencardino J. Normal variants and pitfalls in magnetic resonance imaging of the foot and ankle. In: Shirkhoda A, ed. Normal variations and diagnostic pitfalls in sectional body imaging. Baltimore, Md: Williams & Wilkins, 1999; 641–659.
17. Trevino S, Baumhauer JF. Tendon injuries of the foot and ankle. Clin Sports Med 1992; 11:727–739.
18. Teitz CC, Garret WE, Miniaci A, Lee MH, Mann RA. Tendon problems in athletic individuals. J Bone Joint Surg Am 1997; 79:138–152.
19. Weinstabi R, Stiskal ZM, Neuhold A, Aamlid B, Hertz H. Classifying calcaneal tendon injury according to MRI findings. J Bone Joint Surg [Br] 1991; 73:683–685.
20. Chandnani VP, Bradley YC. Achilles tendon and miscellaneous tendon lesions. Magn Reson Imaging Clin N Am 1994; 2:89–96.
21. Dillon EH, Pope CF, Barber V, Jokl P, Lynch K. Achilles tendon healing: 12-month follow-up with MR imaging (abstr). Radiology 1990; 177(P):306.
22. Bude RO, Adler RS, Bassett DR. Diagnosis of Achilles tendon xanthoma in patients with heterozygous familial hypercholesterolemia: MR vs sonography. AJR Am J Roentgenol 1994; 162:913–917.
23. Rosenberg ZS. Chronic rupture of the posterior tibial tendon. Magn Reson Imaging Clin N Am 1994; 2:79–87.
24. Conti SF. Posterior tibial tendon problems in athletes. Orthop Clin North Am 1994; 25:109–121.
25. Rosenberg ZS, Cheung Y, Jahss MH, Noto AM, Norman A, Leeds NE. Rupture of the posterior tibial tendon: CT and MR imaging with surgical correlation. Radiology 1988; 169:229–235.
26. Khoury NJ, El-Khoury GY, Saltzman CL, Brandser EA. MR imaging of posterior tibial tendon dysfunction. AJR Am J Roentgenol 1996; 167: 675–682.
27. Rosenberg ZS, Beltran J. Magnetic resonance imaging and computed tomography of the ankle and foot. In: Myerson MS, ed. Foot and ankle disorders. Vol 1. Philadelphia, Pa: Saunders, 1998; 123–156.
28. Schweitzer ME, Caccese R, Karasick D, Wapner KL, Mitchell DG. Posterior tibial tendon tears: utility of secondary signs for MR imaging diagnosis. Radiology 1993; 188:655–659.
29. Ouzounian TJ, Myerson MS. Dislocation of the posterior tibial tendon. Foot Ankle 1992; 13:215–219.
30. Bencardino J, Rosenberg ZS, Beltran J, et al. MR imaging of dislocation of the posterior tibial tendon. AJR Am J Roentgenol 1997; 169:1109–1112.
31. Sanmarco GJ. Peroneal tendon injuries. Orthop Clin North Am 1994; 25:135–145.
32. Mota J, Rosenberg ZS. MRI of the peroneal tendons. Top Magn Reson Imaging 1998; 9:273–285.
33. Khoury NJ, El-Khoury GY, Salzman CL, Kathol MH. Peroneus longus and brevis tendon tears: MR imaging evaluation. Radiology 1996; 200:833–841.
34. Schweitzer ME, Eid ME, Deely D, Wapner K, Hecht P. Using MR imaging to differentiate peroneal splits from other peroneal disorders. AJR Am J Roentgenol 1997; 168:129–133.
35. Rosenberg ZS, Beltran J, Cheung Y, Colon E, Herraiz F. MRI of longitudinal splits of the peroneus brevis tendon. AJR Am J Roentgenol 1997; 168:141–147.
36. Rademaker J, Rosenberg ZS, Delfaut EM, Cheung YY, Schweitzer ME. Tear of the peroneus longus tendon: MR imaging features in nine patients. Radiology 2000; 214:700–704.
37. Karasick D, Schweitzer ME. The os trigonum syndrome: imaging features. AJR Am J Roentgenol 1996; 166:125–129.
38. Berger PE, Ofstein RA, Jackson DW, Morrison DS, Silvin N, Amador R. MRI demonstration of radiographically occult fractures: what have we been missing? RadioGraphics 1989; 9:407–436.
39. Lee JK, Yao L. Occult intraosseous fractures: detection with MR imaging. Radiology 1988; 168: 749–750.

40. Lynch TC, Crues JV III, Morgan FW, Sheehan WE, Harter LP, Ryu R. Bone abnormalities of the knee: prevalence and significance at MR imaging. Radiology 1989; 171:761–766.
41. Umans H, Pavlov H. Insufficiency fracture of the talus: diagnosis with MR imaging. Radiology 1995; 197:439–442.
42. McGlone JJ. Stress fracture of the talus. J Am Podiatr Assoc 1965; 55:814–817.
43. Torg JS, Pavlov H, Cooley LH, et al. Stress fractures of the tarsal navicular: a retrospective review of twenty-one cases. J Bone Joint Surg [Am] 1982; 63:700–712.
44. Kathol MH, El-Khoury GY, Moore TE, Marsh JL. Calcaneal insufficiency avulsion fractures in patients with diabetes mellitus. Radiology 1991; 180:725–729.
45. Stafford SA, Rosenthal KI, Gebhardt MC, Brady TJ, Scott JA. MRI in stress fracture. AJR Am J Roentgenol 1986; 147:553–556.
46. Deutsch AL, Mink JH, Waxman AD. Occult fractures of the proximal femur: MR imaging. Radiology 1989; 1709:113–116.
47. Flick AB, Gould N. Osteochondritis dissecans of the talus (transchondral fractures of the talus): review of the literature and new surgical approach for medial dome lesions. Foot Ankle 1985; 5:165–185.
48. De Smet AA, Fisher DR, Burnstein MI, Graf BK, Lange RH. Value of MR imaging in staging osteochondral lesions of the talus (osteochondritis dissecans): results in 14 patients. AJR Am J Roentgenol 1990; 154:555–558.
49. Berndt AL, Harty M. Transchondral fractures (osteochondritis dissecans) of the talus. J Bone Joint Surg [Am] 1959; 41:988–1020.
50. Shelton ML, Pedowitz WJ. Injuries to the talar dome, subtalar joint, and mid foot. In: Jahss MH, ed. Disorders of the foot and ankle. Philadelphia, Pa: Saunders, 1991; 2274–2292.
51. Yulish BS, Mulopulos GP, Goodfellow DB, Bryan PJ, Modic MT, Dollinger BM. MR imaging of osteochondral lesions of the talus. J Comput Assist Tomogr 1987; 11:296–301.
52. Mesgarzadeh M, Sapega AA, Bonakdarpour A, et al. Osteochondritis dissecans: analysis of mechanical stability with radiography, scintigraphy, and MR imaging. Radiology 1987; 165:775–780.
53. Nelson DW, DiPaola J, Colville M, Schmidgall J. Osteochondritis dissecans of the talus and knee: prospective comparison of MR and arthroscopic classifications. J Comput Assist Tomogr 1990; 14: 804–808.
54. Resnick D, Niwayama G. Osteonecrosis: diagnostic techniques, specific situations, and complications. In: Resnick D, Niwayama G, eds. Diagnosis of bone and joint disorders. Philadelphia, Pa: Saunders, 1988; 3238–3288.
55. Haller J, Sartoris DJ, Resnick D, et al. Spontaneous osteonecrosis of the tarsal navicular in adults: imaging findings. AJR Am J Roentgenol 1988; 151: 355–358.
56. Mitchell DG, Kressel HY. MR imaging of early avascular necrosis. Radiology 1988; 169:281–282.
57. Wilson AJ, Murphy WA, Hardy DC, Totty WG. Transient osteoporosis: transient bone marrow edema? Radiology 1988; 167:757–760.
58. Erickson SJ, Quinn SF, Kneeland JB, et al. MR imaging of the tarsal tunnel and related spaces: normal and abnormal findings with anatomic correlation. AJR Am J Roentgenol 1990; 155:323–328.
59. Erickson SJ, Canale PB, Carrera GF, et al. Interdigital (Morton) neuroma: high-resolution MR imaging with a solenoid coil. Radiology 1991; 181: 833–836.
60. Terk MR, Kwong PK, Suthar M, Horvath BC, Colletti PM. Morton neuroma: evaluation with MR imaging performed with contrast enhancement and fat suppression. Radiology 1993; 189:239–241.
61. Jelinek JS, Kransdorf MJ, Utz JA, et al. Imaging of pigmented villonodular synovitis with emphasis on MR imaging. AJR Am J Roentgenol 1989; 152:337–342.
62. Lin J, Jacobson JA, Jamadar DA, Ellis JH. Pigmented villonodular synovitis and related lesions: the spectrum of imaging findings. AJR Am J Roentgenol 1999; 172:191–197.
63. Feldman F, Singson RD, Staron RB. Magnetic resonance imaging in para-articular and ectopic ganglia. Skeletal Radiol 1989; 18:353–358.
64. Beltran J, Caudill JL, Herman LA, et al. Rheumatoid arthritis: MR imaging manifestations. Radiology 1987; 165:153–157.
65. Weishaupt D, Schweitzer ME, Alam F, Karasick D, Wapner K. MR imaging of inflammatory joint diseases of the foot and ankle. Skeletal Radiol 1999; 28:663–669.
66. Kulkarni MV, Drolshagen LF, Kaye JJ, et al. MR imaging of hemophiliac arthropathy. J Comput Assist Tomogr 1986; 10:445–449.
67. Yuh WT, Corson JD, Baraniewski HM, et al. Osteomyelitis of the foot in diabetic patients: evaluation with plain film, ^{99m}Tc-MDP bone scintigraphy, and MR imaging. AJR Am J Roentgenol 1989; 152: 795–800.
68. Beltran J, Campanini DS, Knight C, McCalla M. The diabetic foot: magnetic resonance imaging evaluation. Skeletal Radiol 1990; 19:37–41.
69. Craig JG, Amin MB, Wu K, et al. Osteomyelitis of the diabetic foot: MR imaging-pathologic correlation. Radiology 1997; 203:849–855.
70. Morrison WB, Schweitzer ME, Wapner KL, Hecht PJ, Gannon FH, Behm WR. Osteomyelitis in feet of diabetics: clinical accuracy, surgical utility, and cost-effectiveness of MR imaging. Radiology 1995; 196:557–564.
71. Seabold JE, Flickinger FW, Kao SC, et al. Indium-111-leukocyte/technetium-99m-MDP bone and magnetic resonance imaging: difficulty of diagnosing osteomyelitis in patients with neuropathic osteoarthropathy. J Nucl Med 1990; 31:549–556.
72. Miller TT, Randolph DA Jr, Staron RB, Feldman F, Cushin S. Fat-suppressed MRI of musculoskeletal infection: fast T2-weighted techniques versus gadolinium-enhanced T1-weighted images. Skeletal Radiol 1997; 26:654–658.
73. Berkowitz JF, Kier R, Rudicel S. Plantar fasciitis: MR imaging. Radiology 1991; 179:665–667.
74. Grasel RP, Schweitzer ME, Kovalovich AM, et al. MR imaging of plantar fasciitis: edema, tears and occult abnormalities correlated with outcome. AJR Am J Roentgenol 1999; 173:699–701.
75. Yu JS, Smith G, Ashman C, Kaeding C. The plantar fasciotomy: MR imaging in asymptomatic volunteers. Skeletal Radiol 1999; 28:447–452.